Colorectal Cancer Liver Metastasis Histological Growth Patterns; the Role of the Immune System.

Rafif E. Mattar

Department of Experimental Surgery, McGill University, Montreal

Submitted July 2017.

A thesis submitted to McGill University in partial fulfillment of the requirements of the degree of Master of Science (M. Sc.) in Experimental Surgery.

Table of Contents

Abstract 4
Résumé 6
Dedication 9
Acknowledgments 11
Abbreviations 13
Introduction 14
Colorectal Cancer and Liver Metastases 14
CRCLM Histological Growth Patterns 14
The Immune System 16
The Immune System in CRCLM 17
The Immune System in the HGPs of CRCLM 18
Hypothesis 19
Objectives 20
Methodology 20
Gene Expression Analysis 20
RNA Sequencing and the Study of "Omics" 20
Patient Specimens for Gene Expression Analysis 21
RNA sequencing 21
Data Analysis of Gene Expression Analysis 22
Quantification of T-lymphocytes and Macrophages 23
The Technique of Immunofluorescence 23
Patient Specimens for Quantification of T-lymphocytes and Macrophages 25
Antibodies Used 26
Immunofluorescence Staining Protocol 26
Protocol Optimization and Modification 28
Original Triple Staining vs. Modified Double Staining 29
Image Acquisition 35
Immune Cell Quantification 35
Statistical Analysis for Quantification of T-lymphocytes and Macrophages 36
Results 39
Gene Expression Analysis 39
Heatmaps of Differentially Expressed Genes 39

Canonical Pathways Relevant to each HGP 43
Biological Functions Relevant to each HGP 43
American Association for Cancer Research 107th Annual Meeting 44
Quantification of T-lymphocytes and Macrophages 45
Patient Clinical and Pathological Features Data 45
Immune Cell Populations within the Desmoplastic HGP 46
Immune Cell Populations within the Replacement HGP 48
Comparison of Immune Cell Populations between Both HGPs 50
Overall Infiltration of Immune Cells 54
A Novel Subtype 54
Discussion 55
Transcriptome of Desmoplastic and Replacement CRCLM 56
Immune Cell Populations of Desmoplastic and Replacement CRCLM 58
Conclusions 62
Limitations and Future Directions 63
References 64

Abstract

Background: Colorectal cancer (CRC) is amongst the three most common cancers worldwide with the majority of patients presenting with liver metastases (LM). Resection of liver lesions is the only proven curative measure. Unfortunately, less than 30% of patients are eligible for resection. Three major histological growth patterns (HGPs) have been identified in patients with colorectal cancer liver metastasis (CRCLM); desmoplastic, pushing and replacement. Patients with replacement lesions have a poor overall survival rate compared to those with desmoplastic when treated.

A number of studies have reported that the magnitude and composition of T-lymphocyte infiltration in both the primary and metastatic CRC is significantly correlated with prognosis. High infiltration of tumor associated macrophages (TAM) has also been associated with prolonged overall survival in CRC, and better outcome in CRCLM. Furthermore, the role of these immune components when LM are segregated by HGP has not yet been evaluated thoroughly. Defining this is important in light of the fact that new therapies are based on manipulation of various components of the immune system.

Methodology

Gene Expression Analysis: Samples were obtained through the McGill University Hospital Centre Liver Disease Biobank (MUHC-LDB); 9 Desmoplastic and 6 Replacement lesions. To minimize heterogeneity in the data, we selected chemonaïve samples. Samples were scored with our pathologist collaborators for tumor viability and purity to ensure that select areas fully representative of the HGPs. Tumors were macrodissected, along with adjacent normal liver and processed for RNA-seq. Sequencing was performed by our collaborator Dr. Woong-Yang Park at the Samsung Genome Centre in South Korea, using the illumine HISeq sequencers. R© software was used to identify differentially expressed genes, and to generate heatmaps. From the output of this data, we began studying genes and pathways using Ingenuity Pathway Analysis (IPA©) software.

Immune Cell Quantification: Serial sections of formalin fixed paraffin embedded (FFPE) biopsies from CRCLM of both desmoplastic and replacement HGPs were stained via immunofluorescence, to assess the presence and distribution of various subtypes of T-

lymphocytes and macrophages. Antibodies used were: CD68 (all macrophages), IRF5 (M1 macrophages), CMAF (M2 macrophages). For the T-lymphocyte population: Granzyme B (activated cytotoxic T-lymphocytes), CD4 (helper T-lymphocytes), and FOXP3 (regulatory T-lymphocytes). Tiled images of the whole tissue sections were obtained using a florescent microscope, followed by manual counting of each of the immune cell populations.

Results

Gene Expression Analysis: Significant biological functions between the patterns consisted of those mostly related to cellular processes such as survival and invasion, suggesting that genes differentially expressed are those related to the tumor formation and metastases cascade. Furthermore, various genes that are related to immunological functions are mostly activated in the replacement pattern and conversely undetected in the desmoplastic subtypes.

Immune Cell Quantification: The majority of immune cell populations concentrated at the tumor/liver interface in both growth patterns, whether that be the tumor peripheries, the desmoplastic ring, or the adjacent normal livers. Furthermore, when comparing desmoplastic and replacement patterns, we found that immune cells are mostly higher at the tumor/liver interface of the replacement pattern. We have also identified a rare subtype of immune cells; $CD4^-$ regulatory T-lymphocytes. This population has not yet been described in patients with CRC or with CRCLM**.**

Conclusions: Different components of the immune system play diverse roles in the desmoplastic and replacement patterns of CRCLM. The findings described in this paper are new and will help increase our understanding of the diversity of CRC liver metastases. Such findings can direct future work to identity new prognostic markers and to help future therapeutics development towards therapies that can manipulate various components of the immune system.

Résumé

Contexte: Le cancer colorectal (CRC ; *Colorectal Cancer*) est parmi les 3 cancers les plus répandus dans le monde. La majorité des patients atteints par cette maladie développent des métastases hépatiques (LM ; *Liver Metastasis*). La résection des lésions hépatiques est la seule intervention disponible pour prolonger la survie des patients. Malheureusement, moins de 20% de ces patients sont admissibles à la résection. Trois principaux modèles de croissance histologique (HGP ; *histological Growth Patterns*) ont été identifiés chez les patients atteints de CRCLM, à savoir *Desmoplastic*, *Pushing* et *Replacement*. Suite aux traitements, les patients ayant des lésions de type *Replacement* ont une survie globale moindre comparée à ceux présentant des lésions de type *Desmoplastic*.

Plusieurs études ont rapporté que le niveau et la composition des lymphocytes T infiltrant aussi bien les lésions CRC primaires que métastatiques sont significatives d'un point de vue pronostic. Les macrophages associés à la tumeur (TAM ; *Tumor associated macrophages*) ont également été associés à une survie globale prolongée dans le CRC. Aussi, une infiltration élevée de TAM dans le CRCLM a également été associée à une meilleure issue. Cependant, le rôle de ces composantes immunitaires dans les LM en fonction des différents HGP n'a pas encore été investigué à fond. L'investigation de cet aspect est importante étant donné que les nouvelles voies thérapeutiques s'orientent vers la manipulation de diverses composantes du système immunitaire.

Méthodologie

Analyse de l'expression génique: Les échantillons ont été obtenus de notre Biobanque tissulaire (i.e. *Mcgill University Hospital Centre Liver Disease Biobank (MUHC-LDB)*). Ceux-ci incluent 9 lésions de type *Desmoplastic* et 6 lésions de type *Replacement*. Pour réduire l'hétérogénéité dans les données, nous avons sélectionné des échantillons provenant de patients n'ayant pas reçus de chimiothérapie (i.e. *Chemonaive*). Les échantillons ont été évalués par nos pathologistes quant à la viabilité et la pureté de la tumeur pour s'assurer que les zones à étudier sont représentatives des HGP. Les zones avec le tissu tumoral et celles de tissu hépatique sain ont été récoltées par macrodissection, et apprêtées pour l'ARN-seq. Le séquençage HISeq a été réalisé dans les laboratoires de notre collaborateur Dr. Woong-Yang Park au *Samsung Genome Center* (Corée du Sud), à l'aide des séquenceurs illumine HISeq. Le logiciel R© a été utilisé pour

déterminer l'expression différentielle des gènes, et pour générer des cartes *heatmaps*. En utilisant ces données, nous avons commencé l'étude des gènes et des voies en utilisant le logiciel Ingenuity Pathway Analysis (IPA©).

Quantification des cellules immunitaires: Pour évaluer la présence et la distribution de divers sous-types de lymphocytes T et de macrophages, des sections sériées de lésions CRCLM en paraffine (FFPE ; *formalin fixed paraffin embedded*) de types *Desmoplastic* et *Replacement* ont été marquées pour des analyses par immunofluorescence. Nous avons utilisé des anticorps contre les marqueurs suivants : CD68 (les macrophages totaux), IRF5 (les macrophages M1), CMAF (les macrophages M2), Granzyme B (les lymphocytes T cytotoxiques activés), CD4 (les lymphocytes T auxiliaires) et FOXP3 (les lymphocytes T régulateurs). Des images de l'ensemble des coupes tissulaires ont été captées à l'aide d'un microscope à fluorescence, suivi d'un comptage manuel de chacune des populations de cellules immunitaires.

Résultats

Analyse de l'expression génique: Les différences significatives entre les différents patrons HGP sont celles qui sont principalement liées aux processus cellulaires tels que la survie et l'invasion. Ceci suggère que les gènes exprimés de façon différentielle sont ceux liés à la formation de la tumeur et à la cascade métastatique. En outre, divers gènes reliés aux fonctions immunologiques sont principalement activés dans les lésions de type *Replacement*, alors qu'ils sont absents dans les lésions de type *Desmoplastic*.

Quantification des cellules immunitaires: Dans les 2 types de patrons de croissance (*Desmoplastic* vs. *Replacement*), nous avons observé que l*a* majorité des populations de cellules immunitaires se concentrent au niveau de l'interface tumeur/tissu hépatique, et ceci que ce soit la périphérie tumorale, le disque desmoplastique (*Desmoplastic Ring*) ou le tissu hépatique sain adjacent. En outre, en comparant les types *Desmoplastic* et *Replacement*, nous avons observé que le nombre des cellules immunitaires est plus élevé au niveau de l'interface tumeur/tissu hépatique les lésions de type *Replacement*. Nous avons également identifié un sous-type rare de cellules immunitaires (des lymphocytes T régulateurs $CD4^-$) ; une population de lymphocytes qui n'a pas encore été décrite dans les CRC et les CRCLM.

Conclusions: Il ressort que différentes composantes du système immunitaire jouent des rôles distincts dépendamment des patrons *Desmoplastic* et *Replacement* des métastases hépatiques du CRC. Une revue de la littérature, nous laisse croire que nous sommes les premiers à rapporter ces résultats intéressants. Certes, ces résultats aideront à mieux comprendre la diversité des métastases hépatiques. Nous espérons pouvoir améliorer l'état de nos patients en identifiant ceux qui pourront profiter le plus des thérapies qui ciblent les différentes composantes du système immunitaire.

Dedication

First and foremost, I'd like to thank Allah (God), for I have always and forever been graced by his multiple blessings.

One of Allah's greatest gifts to me has been my loving fiancé, Faisal Al-alem. Faisal I thank you whole heartedly for supporting me throughout this journey. You've stood beside me and encouraged me from the moment I met you. Without you, I would not have had the power to travel half way across the world to pursue this masters. I know you have sacrificed a lot. Despite the enormous time difference, you've listened to my daily updates, brainstormed with me, gotten excited about my achievements, and even sat down to help me find solutions each and every time I thought I'd hit a wall. I continue to learn from you every day. Your pure belief in me gives me the will to keep on going. Faisal, I am forever grateful for your presence in my life.

To my parents, Lina Hammad and Essam Mattar. You ignited the inquisitive flame within me at a very young age. Mum, our weekly trips to the library made we want to "write a sentence" of my own, to be the person who discovered something vital to human knowledge. You both taught me what true passion for one's profession looks like. I've spent hours as a child and now as an adult admiring your devotion. Thank you for teaching me that even if the road is long, if you endure it in the correct way, you will gain so much. Your prayers and pearls of wisdom each time I call home, make the journey worth it. I am proud to be your daughter. Mum, Dad, I owe you the world.

To my younger siblings, Rahif, Reef, Abdulraouf, and Raeef. Your smiles and cheers over the phone always make things easier and brighter. Thank you for nagging me to sit down and work when I didn't feel like it. Boys, although I know how excited you get when I visit home, your refusal to play card games with me until I'd finished work for the day, makes me realize how caring and kind you've grown up to become.

To my grandparents, Faridah Rifai and Fahmi Hammad. I can feel how proud you are of me each time I call or share a photo. Your applaud and prayers lift my spirit up each and every time.

To my late grandparents, Nour Etergy and Hussain Mattar. My father has shared with me the words of advice you would gift him when he was in my shoes. These words will always guide me when I need them most.

To my sisters in law, Hala and Sahar, I'm very fond of our writing gatherings around the kitchen table. They always made the work seem a little less painful.

Last but not least, to my mentor and co-supervisor Dr. Mazen Hassanain. A few years back, in my final year of medical school in Saudi Arabia, you introduced me to the world of surgical research. Until that point in time, I'd sworn that I wouldn't work on basic science nor oncology; I thought one was boring and the other was depressing. Thank you for making me realize that I was wrong. Thank you for providing me with opportunity upon opportunity to flourish. Throughout the years you've lent an understanding ear, and given me advice on both my work and life. I will always be thankful for your care, guidance, and support.

To each of you, I dedicate this thesis.

Rafif, July 2017.

Acknowledgments

I'd like to thank my family and friends for supporting me unconditionally, gifting me their sincere encouragement and advice, and making this trip so far away from home worthwhile.

I would like to thank King Saud University, Riyadh and the Saudi Arabian Cultural Bureau in Canada for granting me a scholarship to pursue this masters, and for their continuous support.

I thank the members of the lab, Dr. Anthoula Lazaris for your guidance and help throughout the project, and Lotfi Amri for showing me the way around the lab, teaching me to stain, and providing me with samples.

I am also grateful to Dr. Woong-Yang Park and his team at the Samsung Genome Institute for their collaboration on the RNA-seq experiments, and for kindly providing us their expertise and continuous support.

I am humbled with gratitude to my friends and colleagues, Dr. Hadeel Jallad for helping me optimize my protocol when I was ready to give up. Dr. Min Fu from the core imaging facility for spending many hours with me viewing my slides and brainstorming ways to better them. Dr. EunJoo (Julie) Lee and Anna Perez for teaching me how to use the florescent microscope. Dr. Pablo Zoroquiain for providing your opinion as a pathologist and reviewing the H&E slides with me. Dr. Mohamed Abdouh for your advice while I began learning immunofluorescence staining, and for kindly translating my abstract into French. Dr. Yasser Abdulkarim for teaching me how to perform my statistical test. My lab mate Dr. Hussam Alamri for showing me my way around when I first arrived, teaching me how to analyze my data on R©, and providing your opinion on my IF stains. Dr. Zu-hua Gao, Dr. Eleonora Scarlata, Dr. Miguel Burnier Jr, Dr. Ana Beatriz Toledo Dias, Dr. Tommy Nilsson, and Dr. Panina Brodt for allowing me to borrow your materials. My lab mate Nisreen Ibrahim for giving me various tips and tricks. Dr. Roni Rayes for viewing my staining and giving me advice on optimization. Georgia Stavrakis for sharing her knowledge on the basics of immunology. My lab mate Vincent Palmieri and friends Aala Moamar, Dr. Walaa Al-ahmadi, Najat Binothman for helping me out during my experiments.

I would like to express my appreciation to our program coordinator, Ms. Sharon Turner, whose support, guidance, and enthusiasm has made this journey a lot easier. Your quick replies and tolerance to my one thousand and one questions has always put my mind at ease.

I am thankful to the members of my research advisory committee, Dr. Lisbet Haglund, Dr. Jonathan D. Spicer, and Dr. Jacques Lapointe for your guidance which allowed this thesis to come to light.

I am also in debt to Dr. Rabih Halwani, my thesis examiner, for taking time out of his busy schedule to review my thesis. You have provided me with invaluable thoughts and comments, allowing me to present my work in the best way possible.

Finally, to my supervisor Dr. Peter Metrakos, I thank you for providing me with the opportunity to work in your lab, to pursue this masters, and to learn so much more than I'd ever expected.

Abbreviations

BSA	Bovine Serum Albumin
CRC	Colorectal Cancer
CRCLM	Colorectal Cancer Liver Metastases
CTL	Cytotoxic T-Lymphocytes
CTLA4	Cytotoxic T-Lymphocyte Antigen 4
ddH_2O	Double Distilled Water
DN	Desmoplastic Normal Liver
DT	Desmoplastic Tumor
FBS	Fetal Bovine Serum
FFPE	Formalin Fixed Paraffin Embedded
GZB	Granzyme B
H&E	Hematoxylin and Eosin
HGP	Histological Growth Patterns
IF	Immunofluorescence
IHC	Immunohistochemistry
IPA®	Ingenuity® Pathway Analysis
LM	Liver Metastases
MAM	Metastasis-Associated-Macrophages
MSK	Memorial Sloan-Kettering
MUHC	McGill University Health Centre
PBS	Phosphate Buffered Saline
PD-1	Programmed cell Death protein 1
PD-L1	Programmed cell Death Ligand 1
RN	Replacement Normal Liver
RT	Replacement Tumor
RTº	Room Temperature
TAM	Tumor-Associated-Macrophages

Introduction

Colorectal Cancer and Liver Metastases

Colorectal cancer (CRC) is amongst the three most common cancers in many countries [1, 2]. Near two thirds of patients will develop distant metastases during the course of their illness [3]. The liver being the most common site of metastases [3], is also the first and only area of spread in 30-40% of patients [4-6]. The metastases may be either synchronous (developed within 12 months of diagnosis) or metachronous (developed after 12 months of diagnosis). In either case, survival of patients with Colorectal Cancer Liver Metastases (CRCLM) is dismal if left untreated, with a 5-year survival of merely 3.3% for synchronous metastases and 6.1% for metachronous [7]. Yet, unlike many other types of solid organ cancers, the presence of distant metastases does not preclude curative treatment. With ongoing advancements, surgical resection of CRCLM has demonstrated improvement in long-term survival for a significant number of patients, reaching an overall 5-year survival of up to 50-60% [8-10]. Unfortunately, less than 20% of patients are eligible for resection [11], either due to the status of their hepatic or extrahepatic disease, or their overall functional condition. Nevertheless, the criteria for selection of patients for colorectal liver metastasectomy are undergoing continuous modification and expansion [12]. Multimodal management, notably the addition of various regimens of chemotherapy and biological agents, has allowed further prolongation of survival following hepatectomy. To further improve survival, proper selection of patients who would benefit most from such an invasive procedure becomes vital [13].

CRCLM Histological Growth Patterns

Traditionally CRC was staged according to the TNM system, which takes into account T; the size of the tumor, N; number of positive lymph nodes, and M; metastasis status. However it was noticed that postoperative outcomes differed tremendously among patients of the same stage [14]. Consequently, CRCLM have always been approached as a unified entity, although it is not clear why some patients respond to certain regimens, while others do not. Recently, various histological growth patterns (HGP) have been identified amongst CRCLM: desmoplastic, replacement, and pushing [15] (**Fig. 1**) [16]. Desmoplastic lesions were described as being "separated from the surrounding liver parenchyma by a rim of desmoplastic stroma in which, in all cases, a dense lymphocytic infiltrate was present. There was no contact between tumor cells and hepatocytes." Pushing was described as "at the tumor–liver parenchyma interface, the tumor

pushed the liver plates aside which ran in parallel with the circumference of the metastases. There was no desmoplastic stroma formation and the tumor cells were separated from the hepatocytes by a thin layer of reticulin fibers. A mild inflammatory infiltrate was nearly always present at the interface." Finally, replacement lesions were described as "tumor cells were replacing hepatocytes in the liver plates. There was no inflammation and no fibrosis. Tumor cells and hepatocytes had intimate cell–cell contact." This stratification of lesions based on their pattern expands our understanding of the different responses observed clinically; a large collaborative study from our group showed that patients with desmoplastic lesions when treated with chemotherapy plus bevacizumab had a longer survival than did patients with replacement lesions. Where in fact those with a replacement pattern seemed to do worse when bevacizumab was added to their regimen [16].

Figure 1. [16] Diagrams and H&E staining illustrating the morphology of normal liver or the morphology of the tumor/normal liver interface in human CRC liver metastases with a desmoplastic, pushing or replacement HGP.

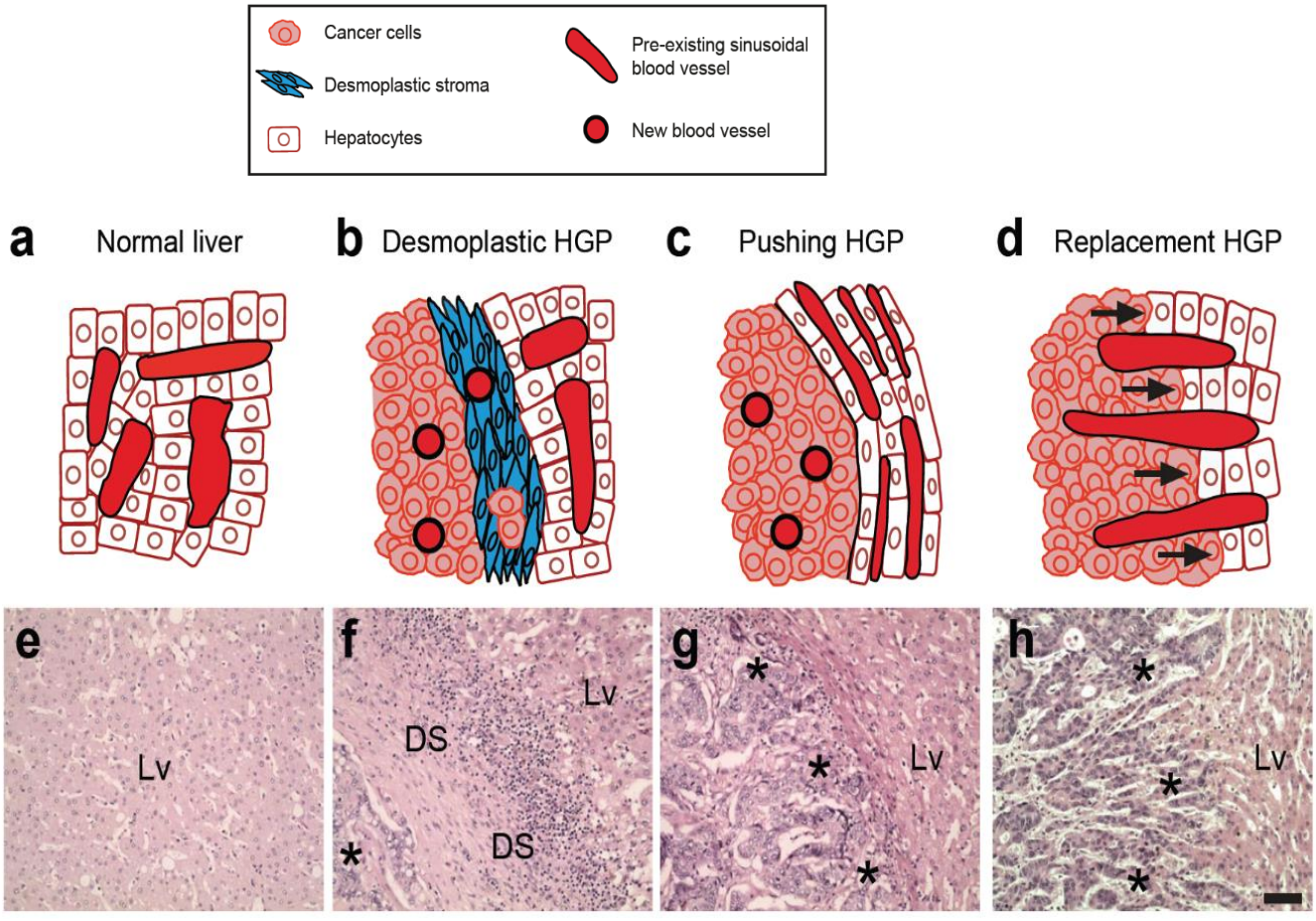

The Immune System

For long, cancer research has focused on the biology of the tumor itself. More recently light has been shed on the role that the host plays; by providing an appropriate niche for tumor formation and metastasis. The immune system specifically serves various diverse purposes in this regards, which differs between immune cell subtypes, as well as between the stages of cancer progression. On histological examination, it is clear that the immune system plays a key role in the difference between each HGP of CRCLM, namely desmoplastic tumors which appear to be surrounded by a lymphocytic infiltrate, which is interestingly near absent in the replacement type (**Fig. 1**) [16].

Functionally, the immune system can be divided into the innate and adaptive immune system. The innate system serves as a first responder to stop the entrance and spread of foreign agents. Macrophages are a component of this system. On the other hand, the adaptive immune system is called upon to react to and clear the unwanted agent. It also provides the body with a specific immunological memory, which allows a much faster and stronger response in the event of a repeat invasion of the harmful agent. T-lymphocytes are a part of the adaptive system [17, 18]. T-cells differentiate to play various interconnected roles; including selective recognition of cellular peptides, direct recognition and killing of antigen expressing cells via cytotoxic T-lymphocytes (CTL), also known as $CD8^+$ effector T-cells, as well as their capacity to orchestrate a multitude of immune reactions via $CD4^+$ helper T-cells. An interesting subset of T-cells are regulatory T-lymphocytes, which as their name implies, regulate and suppress harmful activation of the immune system, thus maintaining self-tolerance and preventing autoimmunity [19-22]. Macrophages serve to maintain healthy tissue by clearing dead cells and foreign materials through phagocytosis, in addition to wound healing through repair and remodeling of tissues [23-26]. Macrophages also play a connecting role between the innate and adaptive immune systems, monitoring their environment then secreting appropriate chemokines and cytokines to trigger and regulate various subsequent inflammatory responses [27, 28]. Based on the stimuli they receive, macrophages "polarize" into diverse phenotypic subtypes; the best established is the M1/M2 axis [29-31]. They are termed activated (M1) and alternatively activated (M2) macrophages. Generally speaking, M1 macrophages secrete pro-inflammatory cytokines, are microbicidal, tumoricidal, and inhibit the fibrotic actions of fibroblasts [32, 33]. M2 macrophages on the other hand, secrete anti-inflammatory cytokines, enhance fibrogenesis, tissue remodeling, and angiogenesis [33-36].

The Immune System in CRCLM

This is all and well in the normal functioning body. However when speaking in terms of cancer, each immune cell subtype contributes in an altered fashion, whether that be a desired anti-tumor effect or a deleterious pro-tumor manner. In their original portrayal in the year 2000, Hanahan and Weinberg described 6 hallmarks of cancer [37]. As science rapidly progressed, 11 years later "avoidance of immune destruction" was added as an emerging hallmark, and "tumor-promoting inflammation" was added as an enabling characteristic [38]. The interaction between T-lymphocytes, macrophages and cancer cells is complex. After receiving signals from antigen presenting cells, T-cells mediate an anti-tumor immunity thus killing cancer cells. Immune checkpoints are various inhibitory signals that prevent this T-cell activity, and thus prevent cancer cell killing. Checkpoints include cytotoxic T-lymphocyte antigen 4 (CTLA4), which are upregulated via activated T-cells, and work via a negative feedback to prevent hyper-immune activation in normal situations. Additional checkpoints include programmed cell death protein 1 (PD-1) and it's ligand (PD-L1) [39]. These checkpoints are important targets when addressing anti-tumor immunity. Interestingly, macrophages express both CTLA4 ligands and PD-L1 [40]. In their landmark paper, Naito et al. [41] established that tumor infiltrating cytotoxic lymphocytes within CRC were associated with a better overall survival. A group at Memorial Sloan-Kettering studied T-lymphocytes in CRCLM; they found that a high number of CD8 T-cells and a low number of CD4 T-cells were independent correlates of 10-year survival following CRCLM resection [42]. It is of note that conflicting evidence exists in terms of CD4 T-lymphocytes; the same group later reported that patients with high infiltration of CD4 T-cells exhibited longer survival [43]. They then looked at the emerging regulatory T-lymphocyte (also named $FOXP3^{+}$ tumor infiltrating lymphocytes, based on their classical marker), and reported that a high number of T-regs relative to CD4 or CD8 T-cells predicted poor outcome; suggesting an immunosuppressive role for regulatory T-lymphocytes [43]. Based on the growing breadth of literature, the TNM staging system was refined to include an immunoscore; TNM-I. This took into account both the tumor burden itself, as well as quantifying two lymphocytes populations (cytotoxic and memory) within the center of the tumor in addition to its' invasive margin [44]. When applied to large cohorts, the immunoscore proved that the higher the infiltration of cytotoxic and memory t-lymphocytes, the longer the disease and overall survival.

Tumor-Associated-Macrophages (TAM) and Metastasis-Associated-Macrophages (MAM) are topics of active research in various cancers. Kruse et al. [45] studied liver metastasis in orthotopic syngeneic colon cancer mouse models; they found that macrophages stimulated metastases, while kupffer cells (which are in fact a form of macrophages present in the liver) actually enhanced tumor formation in the liver. Cui et al. [46] observed that as the numbers of TAM in the primary colorectal cancer decreased, the tumor's ability to metastasize to the liver increased. This ability however did not significantly correlate with the absolute numbers of TAM, but with the percentage of each subtype and the ratio between them; liver metastatic ability increased with lower numbers of M1 macrophages, and higher numbers of M2 macrophages, as well with higher ratios of M2/M1. However, similarly to the contrasting literature regarding helper T-lymphocytes (and most scientific evidence in that case), a recent multicenter study reports that high numbers of TAM infiltrating the resected CRCLM correlated with superior survival outcomes.

The Immune System in the HGPs of CRCLM

This breadth of literature clearly highlights the importance of the immune system in CRCLM, and sheds light on the diverse roles of its various components. The contrasting evidence that is continuously reported could be due to the fact that studies generally approach CRCLM as a unified entity. Segregating patient cohorts based on the 3 different HGPs could provide valuable insights on the diversities that we note clinically, and help us to further understand and tailor our patient care. Only a handful of studies have investigated the various immune cell subtypes in the light of these CRCLM HGPs; Nielsen et al. [47] reported in 2014 that the lymphocytic infiltration at the edge of desmoplastic lesions was denser than that at the edge of replacement and pushing lesions. This however did not influence patient survival. A year later, the same group reported that in resected CRCLM of patients that did not receive chemotherapy, there was no difference of T-lymphocytes (CD3) at the tumor margins of each HGP [48]. Whereas the margins of the replacement type had a higher number of macrophages (CD68) than the other patterns.

To our knowledge, no literature yet exists on the various subtypes of T-lymphocytes nor of macrophages in the different HGPs of CRCLM, namely cytotoxic, helper, and regulatory T-lymphocytes. Nor of M1 and M2 macrophages. In this thesis we aim to address this interesting topic.

Hypothesis

The liver initiates an immune response against the developing tumor. We hypothesize that the immunological response within and around the tumor differs between each growth pattern (**Fig. 2**).

Figure 2. The liver initiates an immune response against the developing tumor. We hypothesize that the immunological response within and around the tumor differs between each growth pattern.

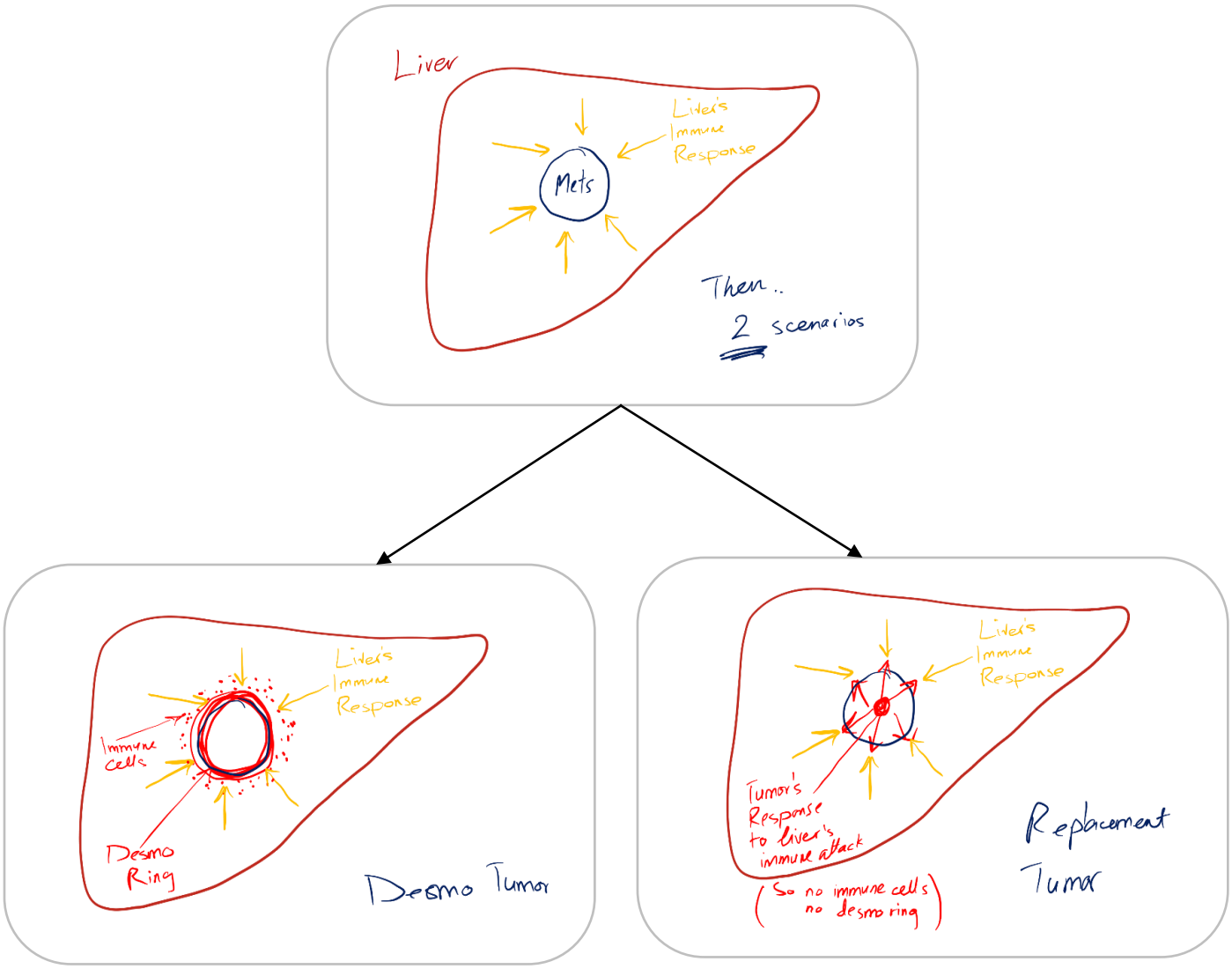

Objectives

We will focus on the desmoplastic and replacement histological growth patterns of CRCLM, as they are the most different. We will study chemonaïve lesions, giving us the advantage of studying the original biology of the tumor and its surroundings. This is of utmost importance, as chemotherapy is known to exert an evident altering effect.

1. To perform gene expression analysis (**RNA Sequencing**) to identify genes, pathways, and functions specific to each growth pattern.
2. To quantify various subtypes of "**T-lymphocytes**" and "**Macrophages**" in each growth pattern via immunofluorescence; namely cytotoxic, helper, and regulatory T-lymphocytes. As well as M1 and M2 macrophages.

Methodology

Gene Expression Analysis

RNA Sequencing and the Study of "Omics"

"Omics" describes the holistic approach to study the biological molecules that make up cells, tissues, and organisms. "Genomics" studies the genome or DNA. "Transcriptomics" studies RNA, or the template that is later translated into protein; this corresponds to the part of the DNA that is actively expressed [49, 50]. While this is a clear advantage, RNA is measured and not the actual protein, and thus must usually be accompanied by some prove of protein expression as validation.

Throughout the years, various methods have been developed to quantify the transcriptome; this includes both hybridization and sequence based methods. Although hybridization approaches are high throughput and are fairly cost effective, they depend on known genomic sequences, and have a high level of background due to cross hybridization [51, 52]. Comparing results from multiple experiments is also difficult using these approaches. As for sequencing based methods that depend on the Sanger technology [53, 54] and directly determine the cDNA sequence, these are usually expensive, and although the newer methods may be high throughput, short tags cannot be mapped to a reference genome.

In recent developments, RNA sequencing (RNA-seq for short) presents itself as a high throughput technology that overcomes many of these limitations. In contrast to hybridization based methods, RNA-seq can detect transcripts that do not correspond to known sequences. It also has near absent levels of background, due to the fact that DNA sequences are mapped to explicit regions of the genome. In addition to this, RNA-seq has limitless quantification, allowing it to detect a vast range of expression levels. Furthermore, owing to the absence of cloning steps, only a small amount of RNA is needed. Finally and most importantly, RNA-seq has a high degree of reproducibility [55, 56]. In the light of this, RNA-seq is the first method that provides high throughput analysis and quantification of the transcriptome. We were able to use this valuable technology to study the different HGPs of CRCLM.

Patient Specimens for Gene Expression Analysis

All samples were procured through the Liver Disease Biobank at McGill University Health Centre (MUHC), Montreal, QC under the direction of Dr. Metrakos. The biobank collects resected specimens and banks both formalin fixed paraffin embedded (FFPE) and snap frozen samples in liquid nitrogen within 30 minutes of resection.

RNA sequencing

Human samples included: 9 desmoplastic and 7 replacement chemonaïve CRCLM snap frozen lesions. 1 replacement lesion was later excluded, as its gene signature looked more like normal liver than that of a tumor. Samples were scored with our collaborator pathologists for tumor viability and purity to ensure that select areas fully representative of the HGPs. Tumors were macrodissected, along with adjacent normal liver and processed for RNA-seq. RNA sequencing and analysis was performed by our collaborator Dr. Woong-Yang Park from the Samsung Genome Centre, Seoul, South Korea. The library construction was performed using Truseq RNA sample preparation v2 kit (Illumina). Quality and quantity of library are measured by Bioanalyzer and Qubit. Sequencing was carried out using the 100-bp paired-end mode of the TruSeq Rapid PE Cluster kit and TruSeq Rapid SBS kit (Illumina) on the HiSeq 2500 sequencing platform (Illumina). The genome reference is hg19 human genome (ver. Jan 2014). TopHat tool (ver2.06) was used for mapping and alignment. The unit of gene counts was count reads.

Data Analysis of Gene Expression Analysis

Analysis was carried out on R (version 3.2.2 - © 2015) [57] and RStudio (version 0.99.489 – © 2009-2015). We chose the "DESeq" package, which uses a method based on the negative binomial distribution, with variance and mean linked by local regression [58]. Groups were labelled as: 1- Desmoplastic Tumors (DT), 2- Desmoplastic Normal (DN), 3- Replacement Tumors (RT), 4- Replacement Normal (RN). Comparison groups were defined as follows: 1- DT vs. DN, 2- RT vs. RN, 3- DT vs. RT, 4- DN s. RN. In other words, tumors from each HGP were compared to their adjacent normal tissues, then tumors of each HGPs were compared to each other, and last, the adjacent normal tissues of both HGPs were compared to each other. Count reads were first normalized. Following this, mean expression, fold changes, log fold changes, p-values, and adjusted p-values were calculated for each comparison group. Finally, heatmaps of the top 30 differentially expressed genes were generated.

Subsequent analysis was performed on Ingenuity® Pathway Analysis (IPA®) software. We are interested in identifying the differences between the desmoplastic and replacement tumors. To achieve this, the following analysis strategy was devised under guidance of a senior scientist from QIAGEN Advanced Genomics Support. First, all 4 comparison groups were injected into IPA. Cut-off values were defined as a p-value < 0.05, no fold change cut-offs were specified. Data was expressed in various methods, we chose to display them in terms of canonical pathways; which determine pathways most significantly affected, as well as those predicted to be activated or inhibited. Next, using the results of the analyses between: "DT vs. DN" and "RT vs. RN", a comparison analysis was performed using an adjusted p-value < 0.05. This allows us to identify pathways distinct to each HGP tumor separately, then to compare pathways between the tumors. This method is more efficient than directly comparing DT to RT, which would only show us the difference between both tumors, without clarifying which pathways were distinct in each separate pattern. Again, data was expressed in various methods, we opted to display diseases and functions that were activated or inhibited in each HGP. IPA uses a right-tailed Fischer Exact test to calculate its p-values.

Quantification of T-lymphocytes and Macrophages

The Technique of Immunofluorescence

Immunofluorescence (IF) is a staining technique that utilizes the concept of antigen-antibody reactions; it relies on labeling target antigens with a florescent dye (also termed fluorochromes), then visualizing them through a florescent microscope (**Fig. 3**). The florescent microscope operates in a similar fashion as a regular light microscope, except that the light source is provided through a laser, which then travels through excitation and emission filters. The excitation filter only permits light that excites the specimen of a certain fluorochrome. The emitted light then passes through the emission filter, which again only allows the specified wavelength to pass to the detector. The emitted photon from the fluorochrome is of a higher wavelength than the exciting photon; this is termed the "stokes shift". This property is an important aspect in florescence labeling and imaging and allows us to differentiate between the exciting and emission light. This information is important when later entertaining the optimization phase specifically of our secondary antibodies, and understanding the different waves explained thereafter.

For decades, patient specimens have been archived in the form of FFPE blocks. This is valuable wealth of knowledge that is continually utilized by the translational research community. Traditionally, the method of Immunohistochemistry (IHC) has been utilized to study these FFPE preserved tissues. It however has major drawbacks, the major one being that IHC is mainly used to label one protein at a time, and when used for multicolor experiments cannot be used to examine co-localization of antigens present in the same cellular compartment. IF on the other hand provides a means of overcoming this by allowing multi-labeling of multiple antigens with different fluorochromes. Traditionally cryopreserved or frozen tissues gave the highest quality labeling by IF, although the architecture of the tissue is somewhat distorted. In FFPE specimens, although tissue architecture is preserved, labeling them via IF has a mantra of its own; the high autofluorescence emitted by these tissues makes detection of labeled proteins problematic. This is unfortunate, because limiting IF to cryosections limits analysis of valuable archived materials. It therefore goes without saying, that finding an applicable technique to utilize the valuable method of IF on the readily available FFPE materials is vital to our understanding of human disease.

Figure 3. Immunoflorescence **(A)** Indirect immunoflorescence is based on an antigen-antibody reaction; the targeted protein is labelled via a primary antibody, which is then recognized by a secondary antibody that is pre-attached to a florescent dye. Image courtesy of © 2007-2017 Sino Biological Inc. **(B)** A florescent microscope is then used to detect the florescence. The florescent microscope operates in a similar fashion as a regular light microscope, except that the light source is provided through a laser, which then travels through excitation and emission filters. The excitation filter only permits light that excites the specimen of a certain fluorochrome. The emitted light then passes through the emission filter, which again only allows the specified wavelength to pass to the detector. Image courtesy of © Leica Microsystems 2017.

A

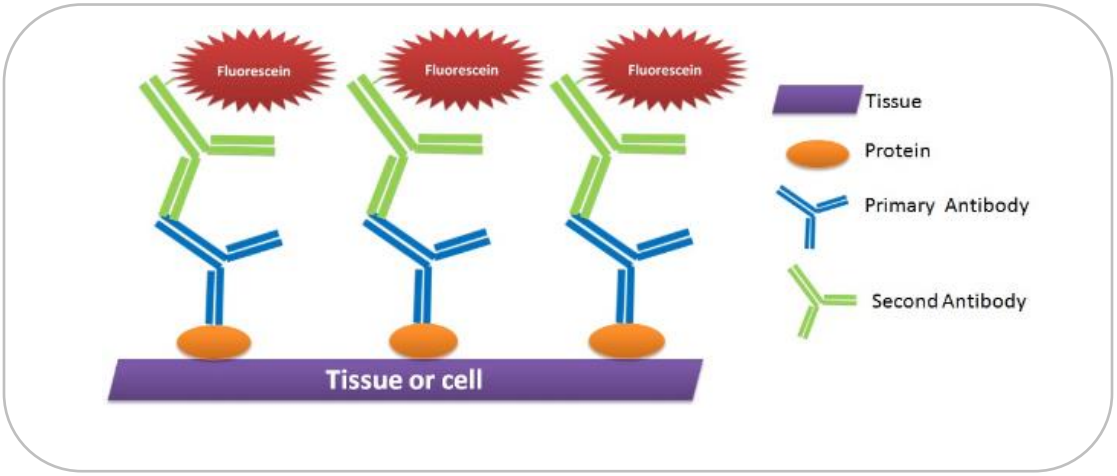

B

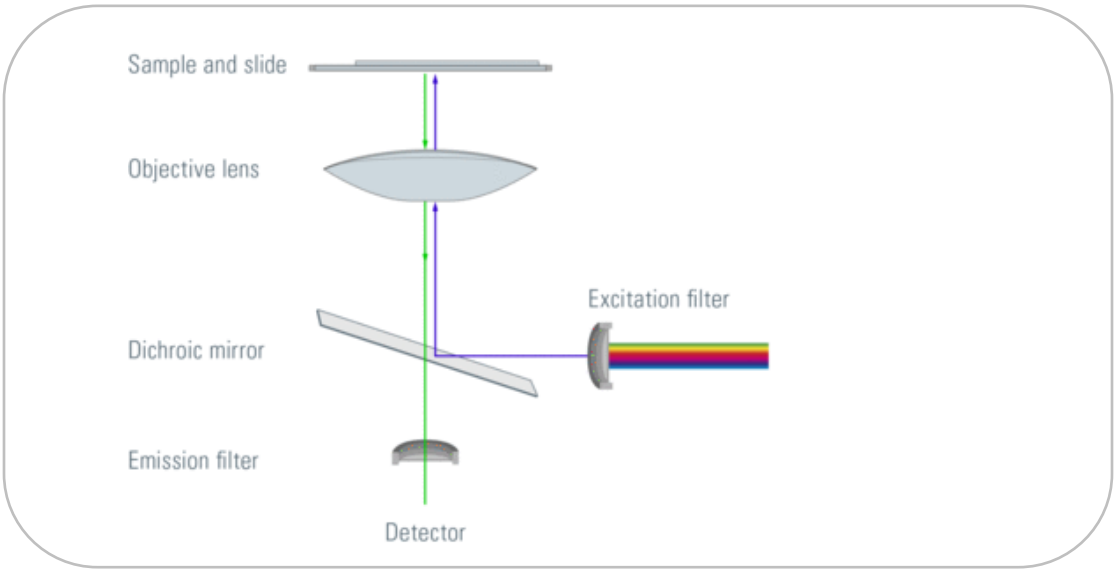

The liver in itself is a highly fluorescent tissue, owing to numerous endogenous fluorophores; NADPH, flavins, reticular fibers, vitamins, bilirubin, lipofuscins, lipopigments, porphyrins, and proteins [59-62]. Despite its traitorous reputation when labeled by IF, tissue autoflorescence can actually be used to distinguish morphology and function. Throughout our experiments on FFPE sections of CRCLM, we were able to optimize our IF protocol to achieve a clear high quality florescent image of multiple labeled immune cells. We also used the liver's autoflorescence to our advantage to define the demarcation between tumor and liver tissue. Additionally, fluorescent images typically only represent a small area of tissue. We were able to capture the image of the whole IF labeled tissue section.

Patient Specimens for Quantification of T-lymphocytes and Macrophages

Specimens of CRCLM were obtained from the department of Pathology at the MUHC. They were processed following resection and stored in the form of FFPE blocks. Sections were cut from each block and stained with hematoxylin and eosin (H&E), then scored by two pathologists to determine the HGP based on the tumor/liver interface as per the criteria described earlier. In our study, we included resected specimens of six patients diagnosed with CRCLM; three were desmoplastic HGP, and three were replacement HGP. All patients did not receive chemotherapy prior to resection. Thus all cancer tissues were chemonaïve. Due to the fact that some lesions had a mixture of different HGPs, lesions with a mixture of HGP and did not have at least 80% of a given pattern were excluded from the study. Clinical data of each patient was also retrieved. Specimens used for quantification of immune cells did not come from the same patients as the specimens used previously for gene expression analysis.

Antibodies Used

Primary antibodies for macrophages:

- CD68 for all macrophages (goat polyclonal, sc7082 Santa Cruz Biotechnology, 1:500).
- IRF5 for M1 macrophages (mouse monoclonal, ab33478 Abcam, 1:200).
- CMAF for M2 macrophages (rabbit polyclonal, sc7866 Santa Cruz Biotechnology, 1:200).

Primary antibodies for T-lymphocytes:

- CD4 for helper T-lymphocytes (mouse monoclonal, ab846 Abcam, 1:50).
- FOXP3 for regulatory T-lymphocytes (goat polyclonal, sc31739 Santa Cruz Biotechnology, 1:50).
- Granzyme B for activated cytotoxic T-lymphocytes (rabbit polyclonal, ab4059 Abcam, 1:200).

Secondary antibodies:

- AF488 donkey anti-mouse (A21202 ThermoFisher Scientific).
- AF488 chicken anti-rabbit (A21441 ThermoFisher Scientific).
- AF594 donkey anti-goat (A11058 ThermoFisher Scientific).
- AF568 donkey anti-rabbit (A10042 ThermoFisher Scientific).

All secondary antibodies were diluted to 1:500.

Immunofluorescence Staining Protocol

Slide Preparation: 4-5 μm serial sections were cut from each FFPE block using a microtome and floated onto a warm water bath (41°C), then picked up onto Fisherbrand™ ColorFrost™ Plus Microscope Slides (12-550-16 Fisher Scientific). They were then put on a vertical rack to air dry, then labeled and transferred to a horizontal rack and left to dry overnight at 37°C in a fan assisted cabinet. Slides were then stored at 4°C until they were needed.

Deparaffinization and Rehydration: On the day of staining, slides were placed in a fan assisted cabinet at 65°C for 1 hour, then left to cool on the bench for 30 minutes. All subsequent steps were carried out at room temperature (RTº). Sections were deparaffinized in 3 washes of xylene

for 5 minutes each. Then rehydrated in graded alcohol; 100% then 94% then 80% for 5 minutes each, and finally washed in double distilled water (ddH_2O) for 5 minutes.

Antigen Retrieval and Permeabilization: A citrate buffer was prepared, its pH adjusted to 6, then 0.05% Tween 20 was added. Sections were immersed in this solution, and put in a vegetable steamer for 10 minutes. They were then put on the bench to cool for 30 minutes. A permeabilization solution was prepared using 0.5% Triton-X100 in 1X PBS. Sections were kept in it for 15 minutes at RTº, and then washed in PBS twice for 5 minutes each.

Immunostaining: The slides around the sections were dried, and using a Mini PAP pen (008877 Thermo Fisher Scientific ®) a hydrophobic barrier was drawn to surround the tissue. This would minimize the volume of solutions used, as well as assuring that the solutions would remain in contact with the tissue sections. All subsequent steps were carried out in a humid dark container, unless otherwise mentioned. A blocking solution was added to each section (2% BSA in 1X PBS, A7030 Sigma). The volumes of materiel used varied between 200-400 µl based on the size of the tissue section. Sections were then placed on a rotating shaker at 20-25 rpm for 1 hour at RTº, then kept flat overnight at 4°C. The following day, the blocking solution was aspirated and each section was washed with 0.1% BSA in 1X PBS for 5 minutes on a rotating shaker at 20-25 rpm. Primary antibodies were diluted in 0.1% BSA in 1X PBS and added to the sections. They were then placed on a rotating shaker at 20-25 rpm for 30 minutes at RTº, then kept flat overnight at 4°C. The next day, primary antibodies were aspirated and each section was washed 3 times with 0.1% BSA in 1X PBS for 5 minutes each on a rotating shaker at 20-25 rpm. Secondary antibodies were diluted in 0.1% BSA in 1X PBS and added to the sections. They were then placed on a rotating shaker at 20-25 rpm for 2 hours at RTº. Secondary antibodies were aspirated and each section was washed 3 times with 1X PBS for 5 minutes each on a rotating shaker at 20-25 rpm. Sections were allowed to dry for 5 minutes in the dark, then 1-2 drops of mountant (ProLong Gold's antifade reagent with DAPI, P36935 Life Technologies) were added, and finally a coverslip (12-5458 Fisher Scientific) was gently placed. Slides were kept to dry horizontally in the dark at RTº overnight. Unless they were visualized the next day, they would then be stored horizontally in the dark at 4°C and visualized within 2 days maximum. After visualization, the edges of each section would be sealed with clear nail polish and stored at -20°C in the dark.

Protocol Optimization and Modification

Antibodies were chosen based on published literature [63-66] and were reviewed by 2 immunologists. The protocol was optimized on various control tissues, including tonsil, spleen and placenta, as they are highly immunogenic. Labeling was also tested on liver tissues from hepatocellular carcinomas and discarded livers that were inadequate for transplant.

Multiple antigen retrieval methods were tested; a glass beacon in a microwave oven, a pressure cooker in a microwave oven, and finally a vegetable steamer was chosen. As for the blocking solution, we experimented with multiple types, combinations, and dilutions of BSA and FBS, and found that 2% BSA that was pure; heat shock fraction, protease free, fatty acid free, essentially globulin free, pH 7, ≥98% (A7030 SIGMA) gave us the least background. The permeabilization step was added later on.

Various titrations of primary and secondary antibody dilutions were tested to find the lowest possible dilutions with the strongest specific labeling. We also tried using different types of buffers to dilute the antibodies; in the beginning we always diluted in the same blocking solution that we used in that experiment. We then elected to use a lower concentration of BSA for our diluting buffer than our blocking buffer (0.1% vs. 2%). Additionally, multiple incubation times were experimented with for the primary antibodies; first we tried 1 hour at RTº, then in another experiment we tried an overnight incubation at 4°C, we finally opted for a combined approach starting with 30 minutes on a rotating shaker at RTº, followed by an overnight incubation at 4°C on a flat surface. As for incubation of the secondary antibody, it was initially for 1 hour, before deciding to increase it to 2 hours on the rotating shaker. It is of note that the use of the rotating shaker was added at a later step, this allowed us to lightly agitate and distribute the volume of solution used.

In regards to the mounting medium, various solutions were tested; a "mowiol" based medium that was prepared in the lab, vs. ProLong Gold's antifade reagent with DAPI (P36935 Life Technologies. We tried adding DAPI to the secondary antibody mix, then to the mowiol mounting medium, before finally choosing to use the ProLong Gold's antifade reagent with DAPI.

Original Triple Staining vs. Modified Double Staining

During the optimization phase, we perfected the single stain for each antibody separately (**Fig. 4**). Following this, we originally intended to proceed to triple staining each HGP with the 3 macrophage markers; CD68, IRF5, and CMAF, in order to find the ratios between unpolarised, M1, and M2 macrophages (**Fig. 5**). And then to separately triple stain with the 3 T-lymphocytes markers; CD4, FOXP3, and GZB, in order to find the ratios between helper, regulatory, and cytotoxic T-lymphocytes (**Fig. 5**). The initial antibody list is attached in (**Table 1**).

Unfortunately, when we actually began triple staining, various bleed through and non-specific staining issues occurred. We thus opted to take 4 serial sections from each FFPE lesion block, and to double stain them as follows (**Fig. 6**):

1. CD68 & IRF5
2. CD68 & CMAF
3. CD4 & FOXP3
4. CD4 & GZB

Figure 4. Optimised Single Stains.

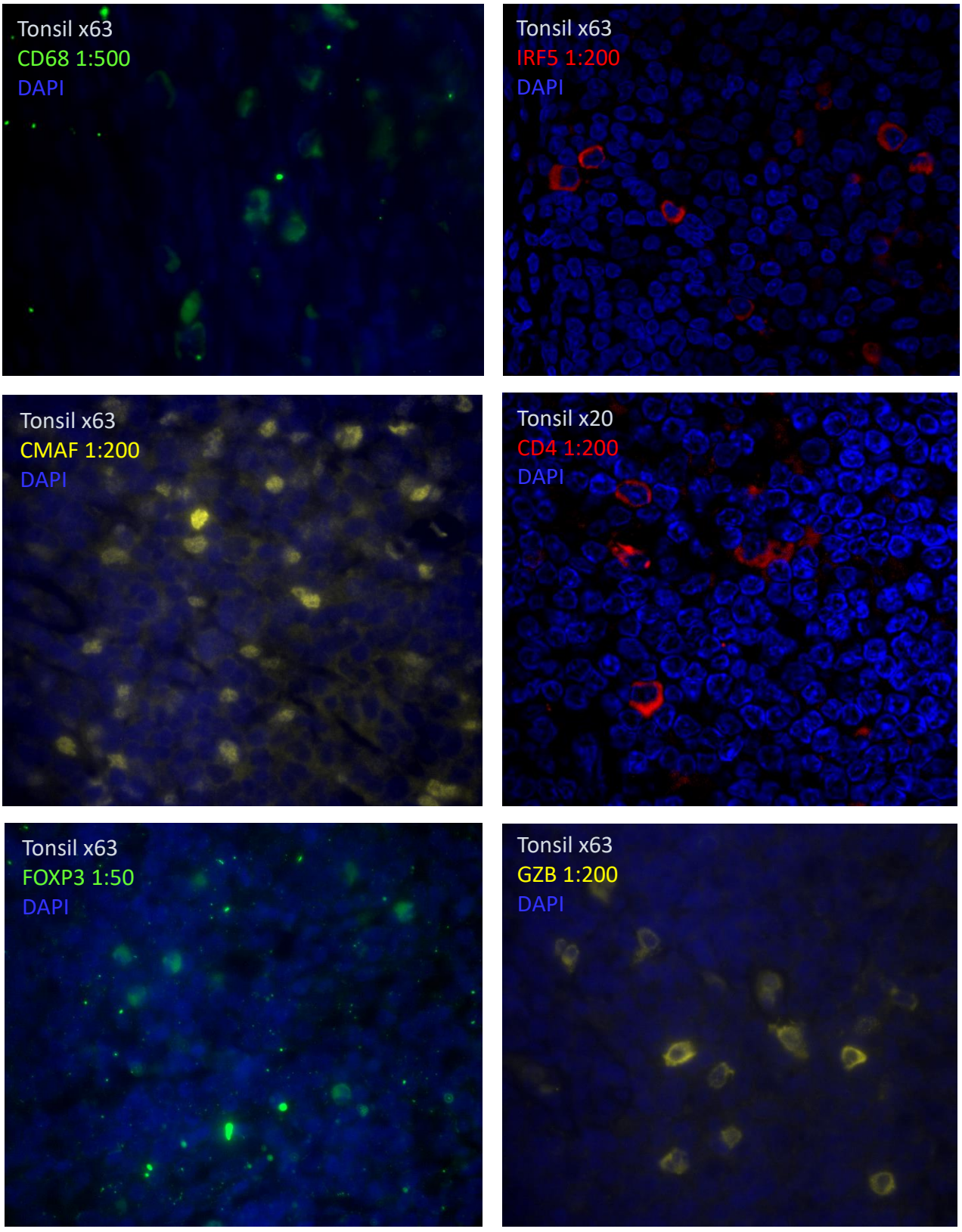

Figure 5. Originial Triple Staning Plan.

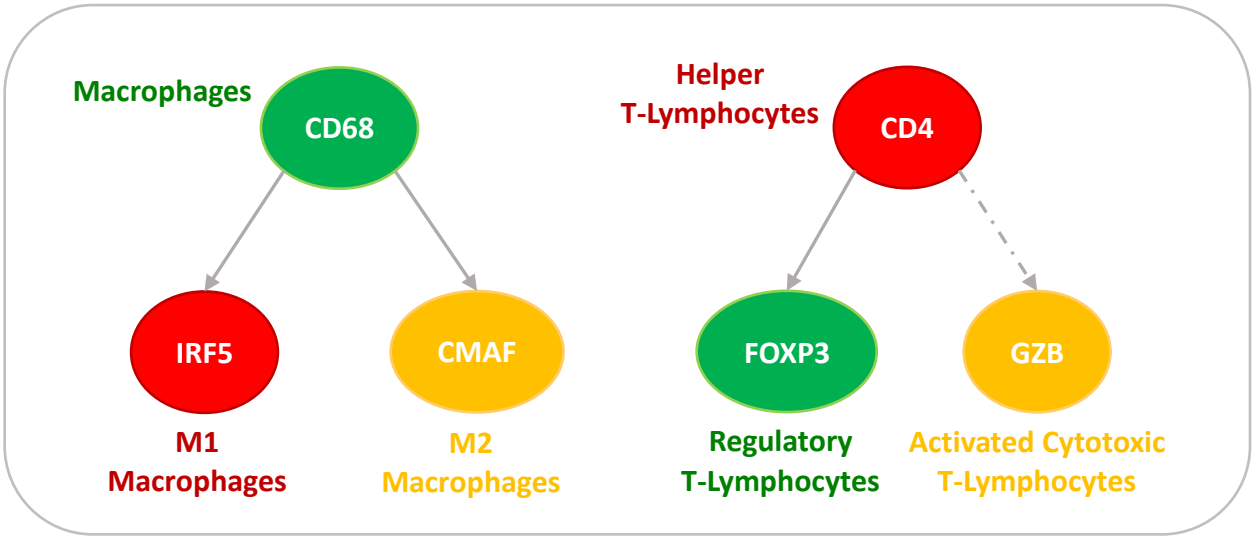

Table 1. Original Antibody List for Triple Staining.

Cell to Stain	Primary Antibody	Cellular Location	Secondary Antibody
All Macrophages	CD68 (goat) 1:500	Golgi vesicles (cytoplasm)	AF488 (donkey x goat) 1:500
M1 Macrophages	IRF5 (mouse) 1:200	Nucleus and cytoplasm	AF647 (goat x mouse) 1:500
M2 Macrophages	CMAF (rabbit) 1:200	Nucleus	AF555 (goat x rabbit) 1:500
Helper T-Lymphocytes	CD4 (mouse) 1:200	Membranous	AF647 (goat x mouse) 1:500
Regulatory T-Lymphocytes	FOXP3 (goat) 1:50	Nucleus (not nucleolus)	AF488 (donkey x goat) 1:500
Cytotoxic T-Lymphocytes	GZB (rabbit) 1:200	Cytoplasmic vesicles	AF555 (goat x rabbit) 1:500

Figure 6. Modified Double Staining Plan.

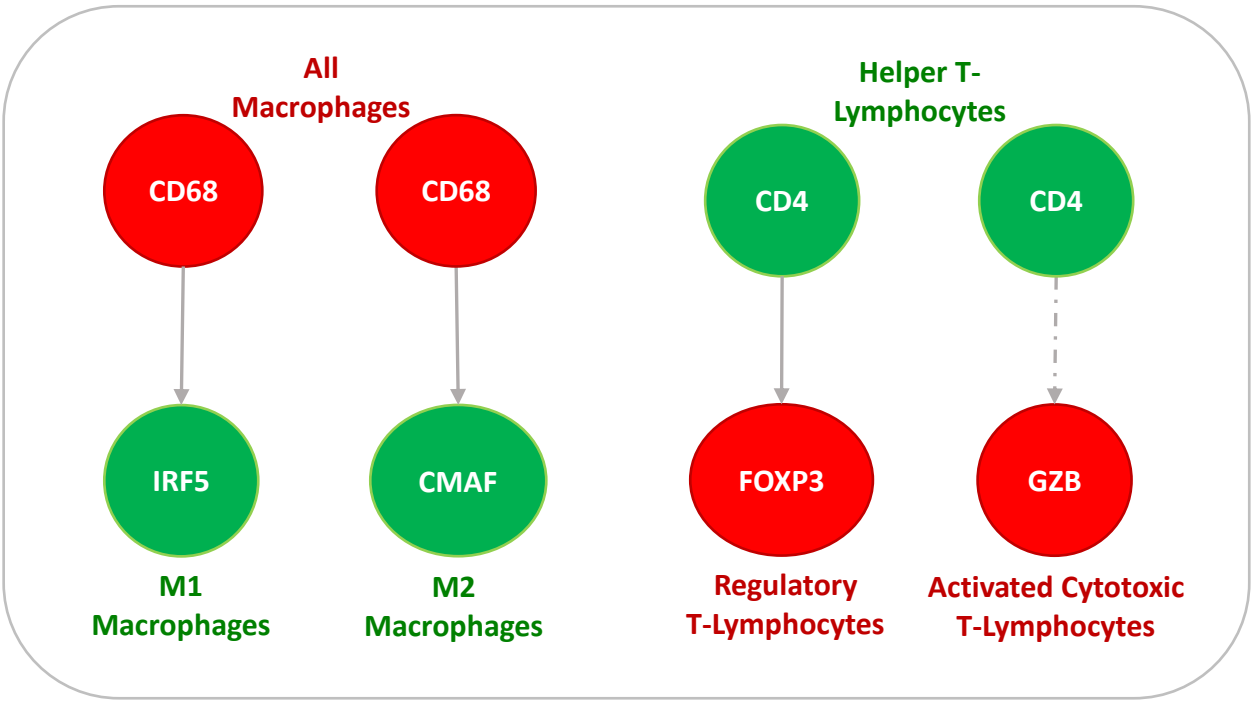

Table 2. Modified Antibody List for Double Staining.

Cell to Stain	Primary Antibody	Cellular Location	Secondary Antibody
All Macrophages	CD68 (goat) 1:500	Golgi vesicles (cytoplasm)	AF594 (donkey x goat) 1:500
M1 Macrophages	IRF5 (mouse) 1:200	Nucleus and cytoplasm	AF488 (donkey x mouse) 1:500
M2 Macrophages	CMAF (rabbit) 1:200	Nucleus	AF488 (chicken x rabbit) 1:500
Helper T-Lymphocytes	CD4 (mouse) 1:50	Membranous	AF488 (donkey x mouse) 1:500
Regulatory T-Lymphocytes	FOXP3 (goat) 1:50	Nucleus (not nucleolus)	AF594 (donkey x goat) 1:500
Cytotoxic T-Lymphocytes	GZB (rabbit) 1:200	Cytoplasmic vesicles	AF568 (donkey x rabbit) 1:500

Asides from converting to a double stain, we used serial sections in order to calculate an approximate ratio between the various immune cell subtypes. We also substituted a number of the secondary antibodies for various reasons (the modified antibody list is attached in **Table 2**): We first eliminated AF647, due to the fact that it is an infra-red fluorochrome and cannot be visualized well on a fluorescence microscope, only on a confocal microscope, making it difficult for us to rapidly check our results. We also had an issue with AF555 as it peaks at a close range to AF488, giving rise to many bleed through issues. We chose to substitute AF555 with AF568 and AF594, both of which peaked farther away from AF488 (**Fig. 7**). Finally, we noticed that some of the secondary antibody species interacted, thus the changes also helped minimize this.

Using this modified plan, double staining was successfully optimized for all antibody combinations. Subsequently, we moved onto experiments with human tissues; 3 desmoplastic lesions and 3 replacement lesions were used. Four serial sections were taken from each, and double stained as mentioned.

Figure 7. Secondary Antibodies Used. (**A**) In the original triple staining plan, AF647 is an infra-red fluorochrome and cannot be visualized well on a florescent microscope. Also, AF555 peaks at a close range to AF488, giving rise to many bleed through issues. (**B, C**) In the modified double staining plan, we chose to substitute AF555 with AF568 and AF594, both of which peaked farther away from AF488, we also eliminated AF647. Images courtesy of © 2016 Thermo Fisher Scientific Inc. N.B The dotted lines are the excitation waves, the solid lines are the emitted "visualized" waves.

A

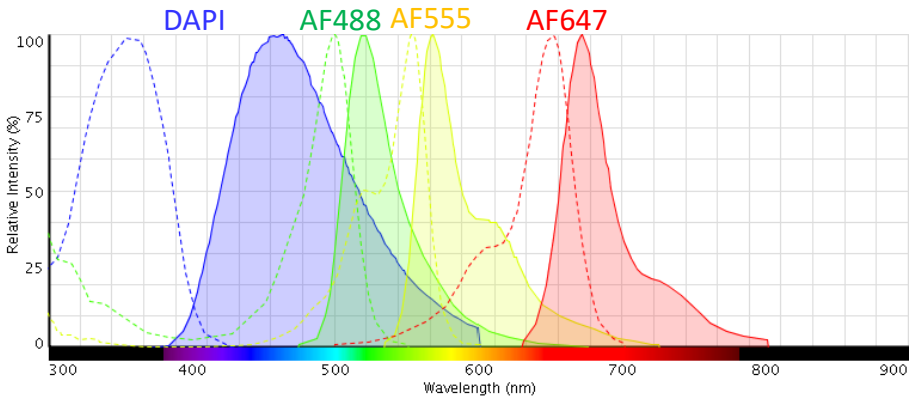

B

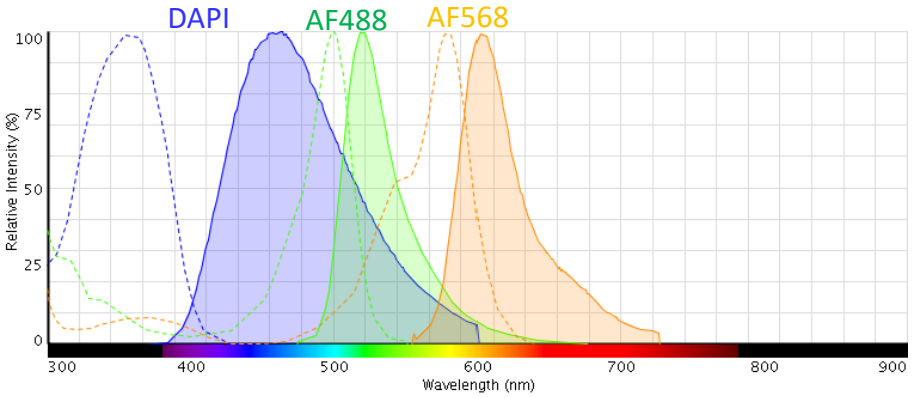

C

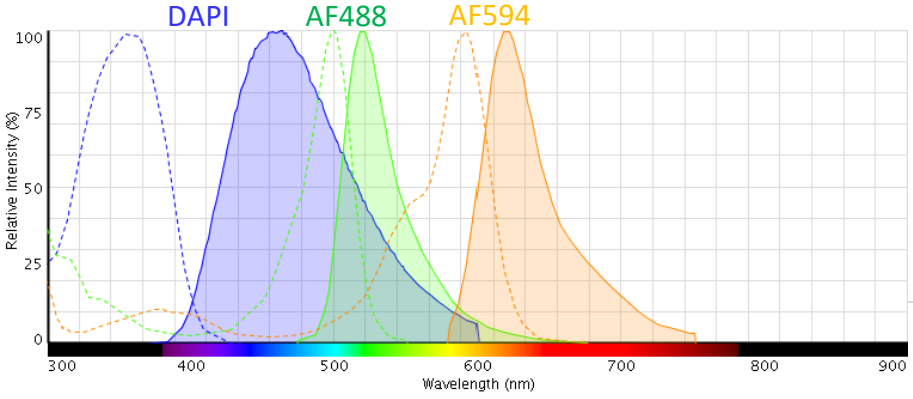

Image Acquisition

Images were acquired using an Axio Imager M2 fluorescence microscope (Carl Zeiss, Germany). A typical image captured by a microscope corresponds to an area of ~0.04mm. We however wanted to image the whole tissue sections, which had an average size of 2*3cm. To do this, we first had to define the borders of the tissue at 5x magnification in a process known as "contouring". The software would then calculate how many "tiles" (a.k.a. images) the microscope needed to take in order to capture the whole section, this ranged between 2500-3700 tiles. We'd then convert to 20x magnification, and refocus the camera in these tiles. To avoid unnecessary exposure of the sections to light, instead of aligning focus point in all ~3000 tiles, we'd realign every ~5 tiles, giving us a total of ~250-350 "focus points". Image acquisition would then commence. Resulting tiles were then stitched and fused using AF488 as the reference color.

Immune Cell Quantification

Before quantification, due to the fact that some lesions were a mixture of different HGP, H&E sections of the same lesions were retrieved and reviewed with the pathologist. Mixed tumor areas and their surroundings were defined. The H&E images were then overlaid onto the florescent images, mixed areas were then demarcated and excluded from further analysis.

Quantification of the florescent labeled images was carried out on ZEN 2.3 software (Blue Edition). © Carl Zeiss Microscopy GmbH, 2011. The mixed areas were first excluded, then each tissue section was divided into regions: (1) central tumor, (2) peripheral tumor, (3) desmoplastic ring (absent in the replacement lesions), (4) close normal liver, (5) far normal liver. Four random areas were chosen in each region, each of an equal size of 209.63*209.63 µm. This allowed us to obtain the final counts as ratios per area, regardless of tumor size. A total of 432 areas were analyzed, 240 from the desmoplastic sections and 192 from the replacement sections. Quantification of each immune cell subtype was carried out manually in each area.

The immune cell populations identified were:

1. $CD68^+$ $IRF5^+$; corresponding to M1 macrophages. (**Fig. 8a**)
2. $CD68^+$ $IRF5^-$; corresponding to all macrophages. (**Fig. 8a**)
3. $CD68^+$ $CMAF^+$; corresponding to M2 macrophages. (**Fig. 8b**)
4. $CD68^+$ $CMAF^-$; corresponding to all macrophages. (**Fig. 8b**)
5. $CD4^+$ $FOXP3^+$; corresponding to $CD4^+$ regulatory T-lymphocytes. (**Fig. 8c**)
6. $CD4^+$ $FOXP3^-$; corresponding to helper T-lymphocytes.
7. $CD4^-$ $FOXP3^+$; corresponding to an emerging and interesting immune cell population; $CD4^-$ regulatory T-lymphocytes. (**Fig. 8c**)
8. $CD4^+$ GZB^+; corresponding to cytotoxic helper T-lymphocytes. (**Fig. 8d**)
9. $CD4^+$ GZB^-; corresponding to helper T-lymphocytes.
10. $CD4^-$ GZB^+; corresponding to activated cytotoxic T-lymphocytes. (**Fig. 8d**)

Comparison Groups: As described above, 5 regions were defined within the desmoplastic sections, and 4 regions within the replacement sections. All 10 immune cell populations were compared between regions within each growth pattern. Then populations were compared between similar regions of both growth patterns.

Statistical Analysis for Quantification of T-lymphocytes and Macrophages

Statistical analysis was performed using the Data Analysis ToolPak from Microsoft ® Excel ®2013. Results are presented as means ± SEM, with the significance value set at $P<0.05$. A Single Factor-ANOVA was used to compare immune cell populations between regions within each growth pattern. A student t-test was used to compare populations between both growth patterns.

Figure 8. Immune Cell Populations Identified. (**A**) Stain of CD68 & IRF5. Cells marked in green are $CD68^{+}$ $IRF5^{+}$; corresponding to M1 macrophages. Cells marked in red are $CD68^{+}$ $IRF5^{-}$; corresponding to all macrophages. (**B**) Stain of CD68 & CMAF. Cells marked in green are $CD68^{+}$ $CMAF^{+}$; corresponding to M2 macrophages. Cells marked in red are $CD68^{+}$ $CMAF^{-}$; corresponding to all macrophages. (**C**) Stain of CD4 & FOXP3. Cells marked in yellow are $CD4^{+}$ $FOXP3^{+}$; corresponding to $CD4^{+}$ regulatory T-lymphocytes. Cells marked in green are $CD4^{+}$ $FOXP3^{-}$; corresponding to helper T-lymphocytes (not shown in here). Cells marked in red are $CD4^{-}$ $FOXP3^{+}$; corresponding to $CD4^{-}$ regulatory T-lymphocytes. (**D**) Stain of CD4 & GZB. Cells marked in yellow are $CD4^{+}$ GZB^{+}; corresponding to cytotoxic helper T-lymphocytes. Cells marked in green are $CD4^{+}$ GZB^{-}; corresponding to helper T-lymphocytes (not shown in here). Cells marked in red are $CD4^{-}$ GZB^{+}; corresponding to activated cytotoxic T-lymphocytes.

A

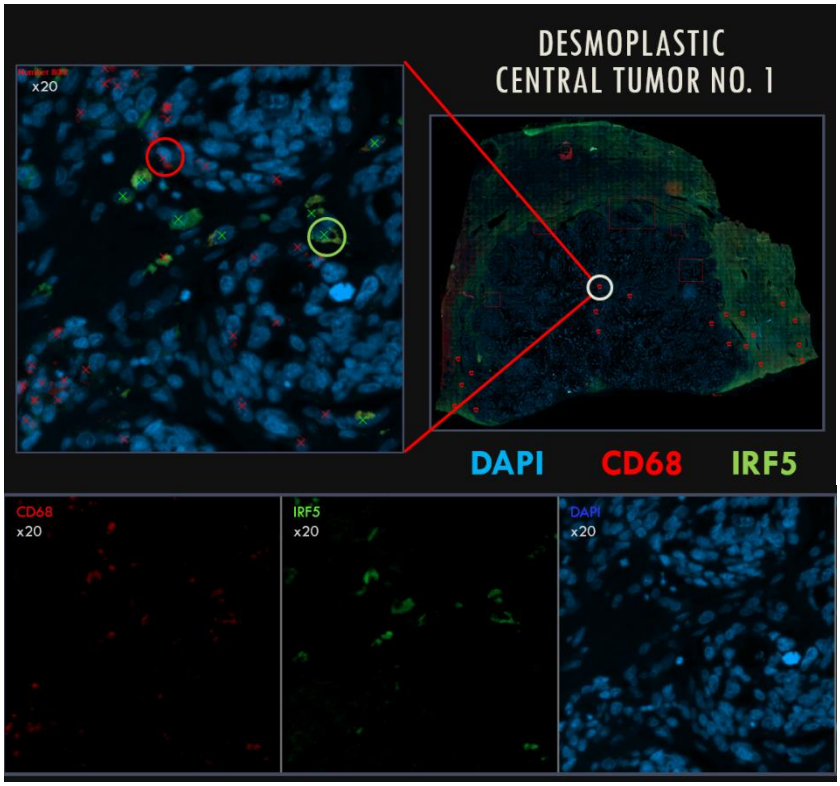

B

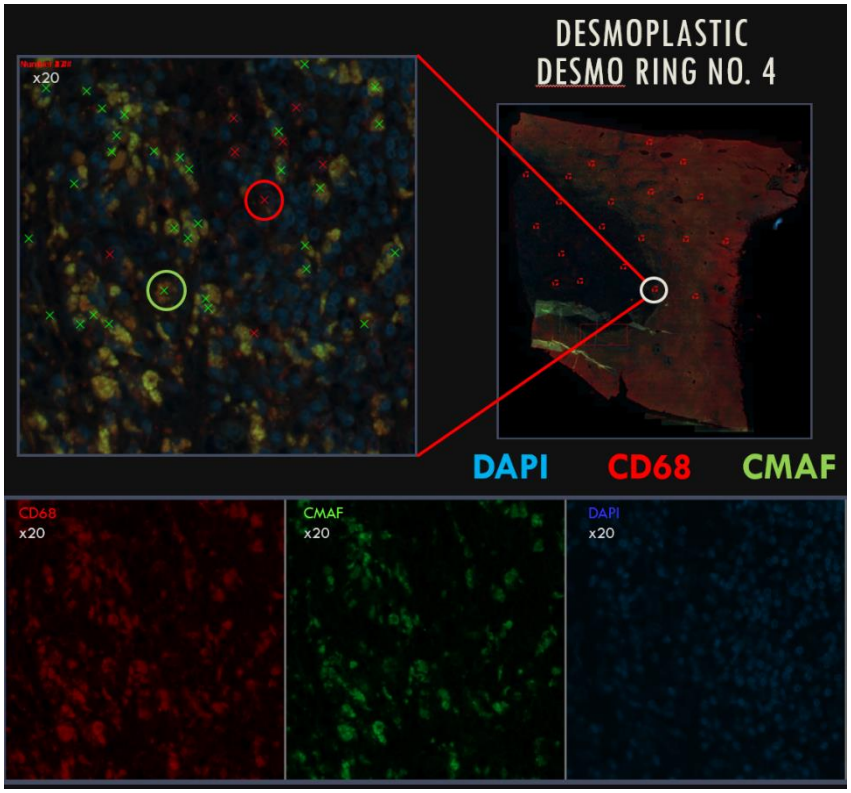
DESMOPLASTIC
DESMO RING NO. 4
x20
DAPI
CD68
CMAF
CD68
x20
CMAF
x20
DAPI
x20

C

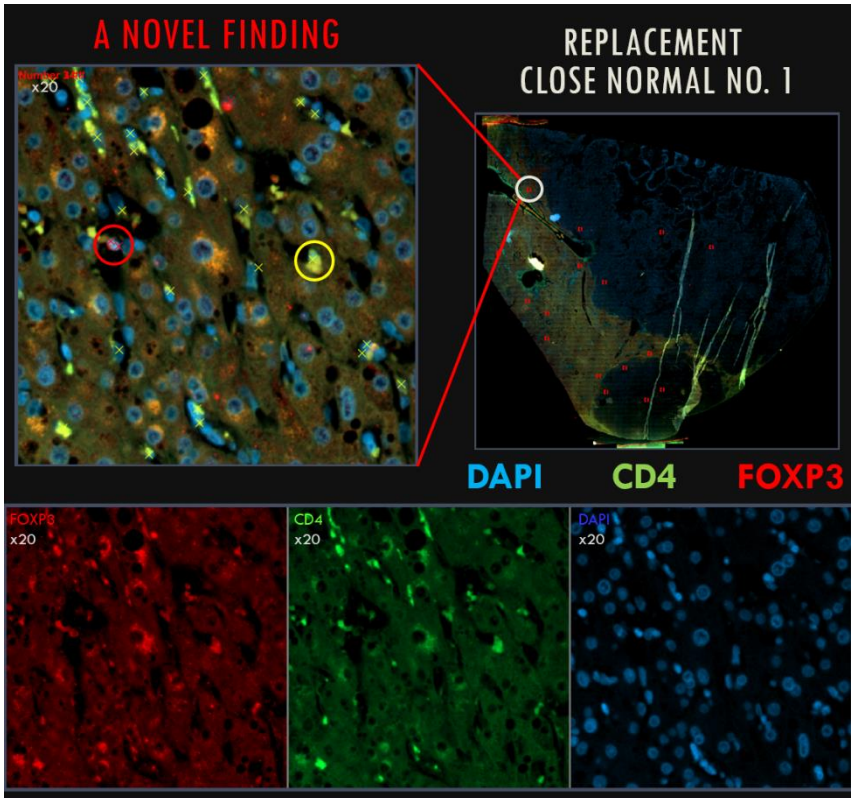
A NOVEL FINDING
REPLACEMENT
CLOSE NORMAL NO. 1
x20
DAPI
CD4
FOXP3
FOXP3
x20
CD4
x20
DAPI
x20

D

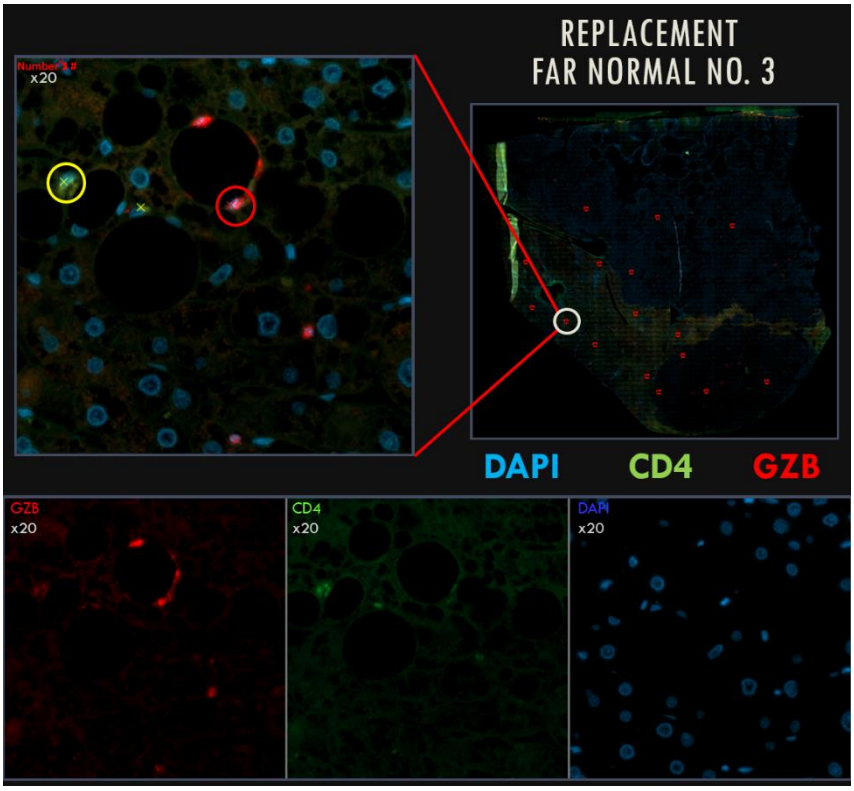

Results

Gene Expression Analysis

Heatmaps of Differentially Expressed Genes

The top 30 differentially expressed genes for each comparison group were displayed in heatmaps via a blinded method. They were arranged both in terms of p-values and gene expression. It is of note, that presenting heatmaps in the gene expression form is much more commonly used, as it groups genes of similar expression patterns. This is useful in our case, as we were able to visualize both similarities and discrepancies within our samples. The p-value form of the heatmaps allows us to first choose the top 30 differentially expressed genes based on p-value, then to group the genes with similar expression together.

RT vs. RN: (**Fig. 9, a-b**) both groups separate out perfectly, whether the genes were arranged based on p-values or gene expression. Some of the genes differentially expressed in the p-value and expression heatmaps are HSD17B13 and TF, respectively; they are both highly expressed in the normal liver samples, in contrast to the replacement tumors where they are very minimal.

DT vs. DN: (**Fig. 9, c-d**) both groups separate out. However, two DT samples seem to form an isolated group when arranged by p-values. The same 2 DT samples cross over into the DN side when arranged by gene expression. Some of the genes differentially expressed in the p-value and expression heatmaps are AKR1C4 and AMBP, respectively; they are both highly expressed in the normal liver samples, in contrast to the desmoplastic tumors where they are very minimal.

RT vs. DT: (**Fig. 9, e-f**) both groups separate out when arranged by p-values. However, the same aforementioned 2 DT samples cross over here as well into the RT side. One of the genes diffrenttially expressed based on p-value is CRP, a known inflammatory marker. In our cohort, is highly expressed in RT in contrast to DT where it is minimal (except for the two DT samples that crossed over). When arranged based on gene expression, there seems to be no clear separation between the replacement and desmoplastic tumors.

RN vs. DN: (**Fig. 9, g-h**) both groups separate out when arranged by p-values. However, one DN sample crosses over into the RN side. When arranged based on gene expression, there seems to be no clear separation between the normal livers adjacent to the replacement and desmoplastic lesions.

Figure 9. Heatmaps of diffrentially expressed genes between various comparison groups: (**A, B**) RT vs. RN: both groups separate out perfectly, whether the genes were arranged based on (**A**) p-values or (**B**) gene expression. (**C, D**) DT vs. DN: both groups separate out. (**C**) However, two DT samples seem to form an isolated group when arranged by p-values. (**D**) The same 2 DT samples cross over into the DN side when arranged by gene expression. (**E**) RT vs. DT: both groups separate out when arranged by p-values. However, the same aforementioned 2 DT samples cross over here as well into the RT side. (**F**) When arranged based on gene expression, there seems to be no clear separation between RT and DT. (**G**) RN vs. DN: both groups separate out when arranged by p-values. However, one DN sample cross over into the RN side. (**H**) When arranged based on gene expression, there seems to be no clear separation between RN and DN.

By p-value

(A)

RT vs. RN

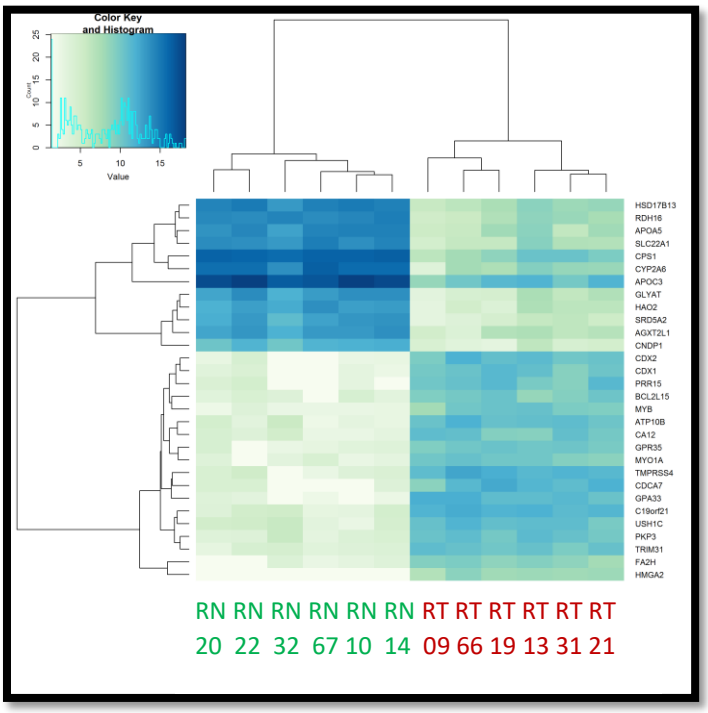

By Gene Expression

(B)

RT vs. RN

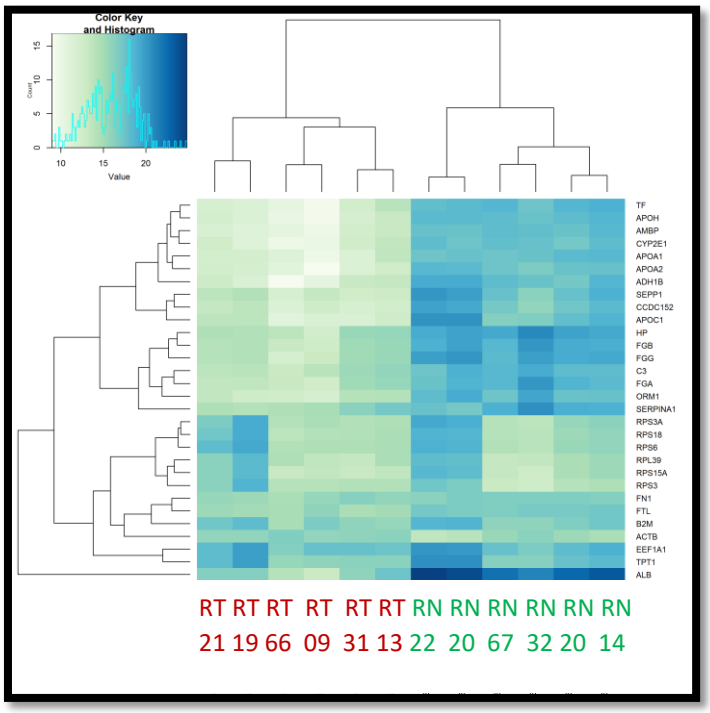

(C)

DT vs. DN

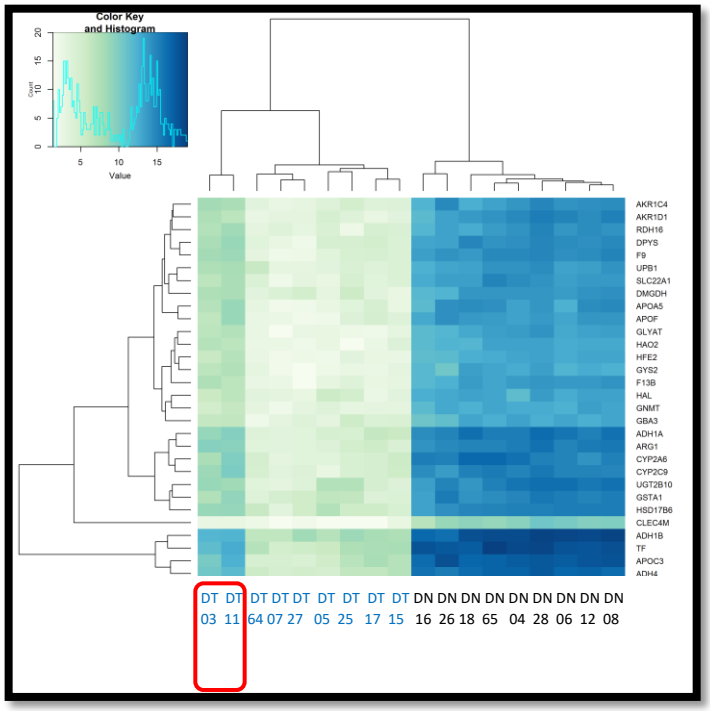

(D)

DT vs. DN

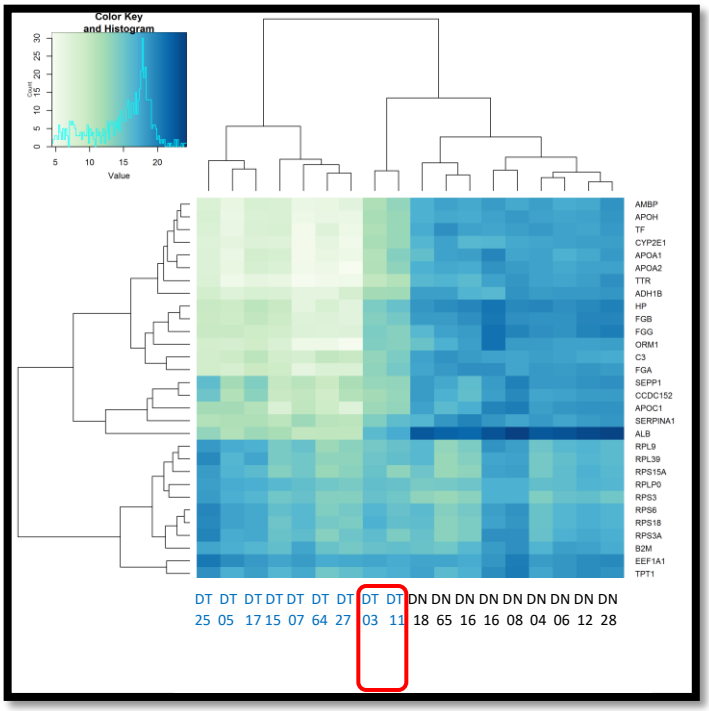

By p-value

By Gene Expression

(E)

RT vs. DT

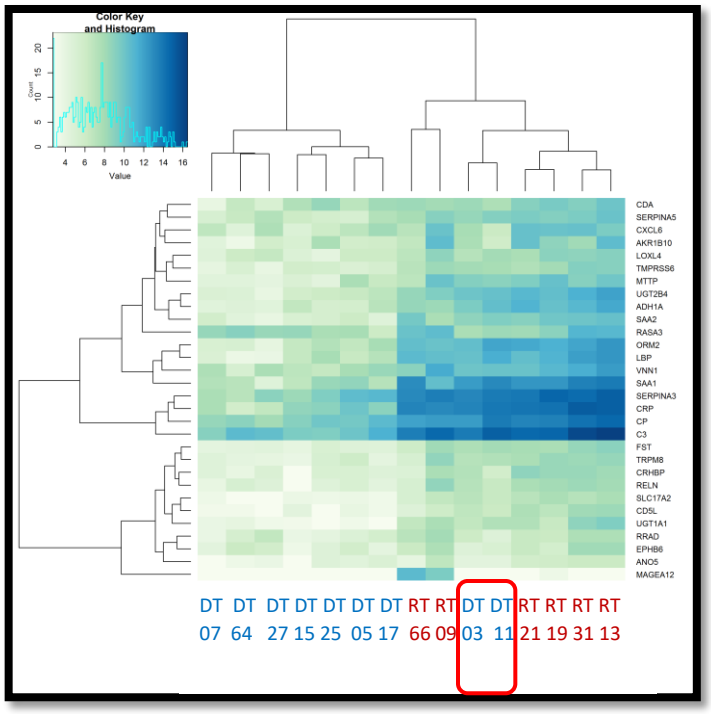

(F)

RT vs. DT

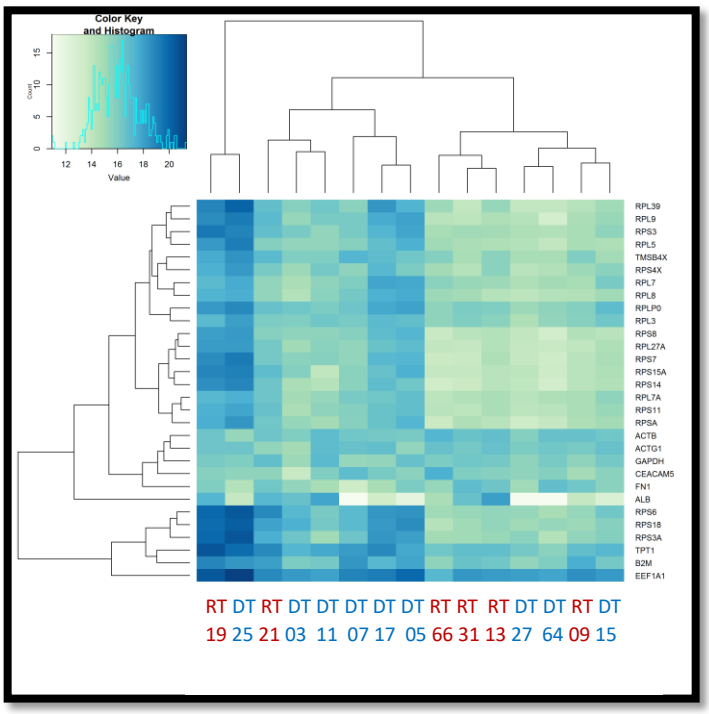

(G)

RN vs. DN

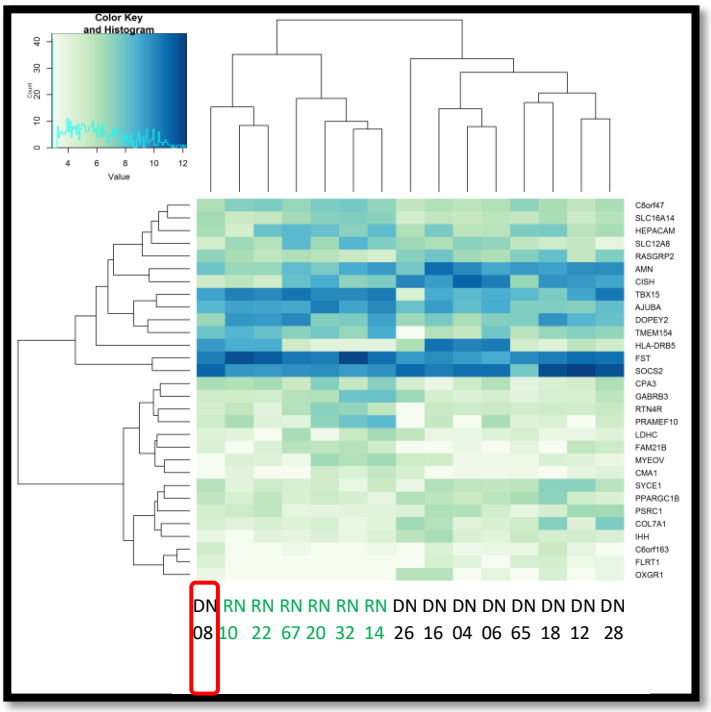

(H)

RN vs. DN

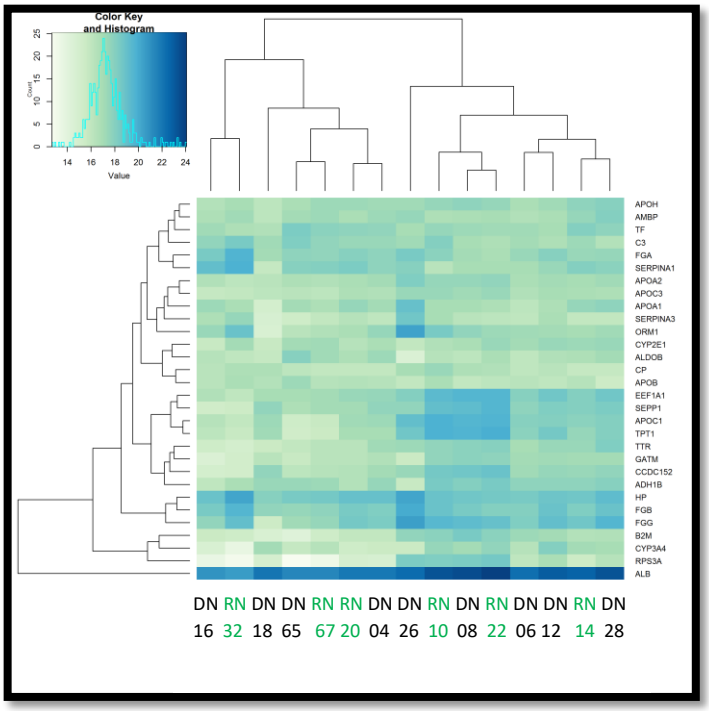

Canonical Pathways Relevant to each HGP

IPA uses QIAGEN's Ingenuity knowledge base data repository, which is created based on millions of biological interactions published in the literature. These are subsequently manually reviewed to assure their accuracy. Canonical pathways describe the most relevant cell signaling and metabolic pathways. Interestingly, no pathways were actually reversed between the 2 HGPs; pathways were either up/down-regulated in both patterns but to a different extent, or absent all together (**Fig. 10**). It is of note that IPA includes all possible pathways, even if they are undetected in the sample. The top 10 relevant pathways between the 2 patterns were: Signaling by Rho Family GTPases, Integrin Signaling, RhoGDI Signaling, Leukocyte Extravasation Signaling, Sperm Motility, Rac Signaling, Aldosterone Signaling in Epithelial Cells, RhoA Signaling, Colorectal Cancer Metastasis Signaling, and Endothelin-1 Signaling. All, but the RhoGDI Signaling pathway, were upregulated.

Biological Functions Relevant to each HGP

Biological functions describe "the biological and disease processes relevant to my genes of interest." (Bioinformatics Unit, Spanish National Cancer Center. 2007). Similarly to the canonical pathways, no biological functions were completely reversed between the 2 HGPs; functions were either up/down-regulated in both patterns but to a different extent, or absent all together. The 10 most relevant functions were cell survival, invasion of cells, proliferation of cells, invasion of tumor cell lines, organismal death, cell viability, cell movement, migration of cells, cell viability of tumor cell lines, and cell movement of tumor cell lines. Again alike the canonical pathways, all of these functions were up-regulated, with the exception of organismal death.

When taking a closer look at immunological related functions, such as leukocyte migration, development and quantity of leukocytes, interestingly they were mostly activated in the replacement pattern and conversely undetected in desmoplastic (**Fig. 11**). This observation led us to our second objective: "To *quantify various subtypes of "T-lymphocytes" and "Macrophages" in each growth pattern; namely cytotoxic, helper, and regulatory T-lymphocytes. As well as M1 and M2 macrophages*."

American Association for Cancer Research 107th Annual Meeting

The RNA-seq data analyzed here was included in a poster presented at the American Association for Cancer Research (AACR) 107th Annual Meeting 2016, held in New Orleans, LA. The presentation was titled: Lazaris A, Amri A, Zoroquiain P, Ibrahim N, Alamri H, Mattar R, Petrillo SK, Gao Z, Vermeulen P, Metrakos P. "*Vascularization of colorectal cancer liver metastasis: correlation with growth patterns.*" [67]

Figure 10. Canonical Pathways relevent in Replacement and Desmoplastic Tumors.

Figure 11. Immunological functions relevant to each HGP. Notice they are mostly activated in the replacement pattern and undetected in desmoplastic.

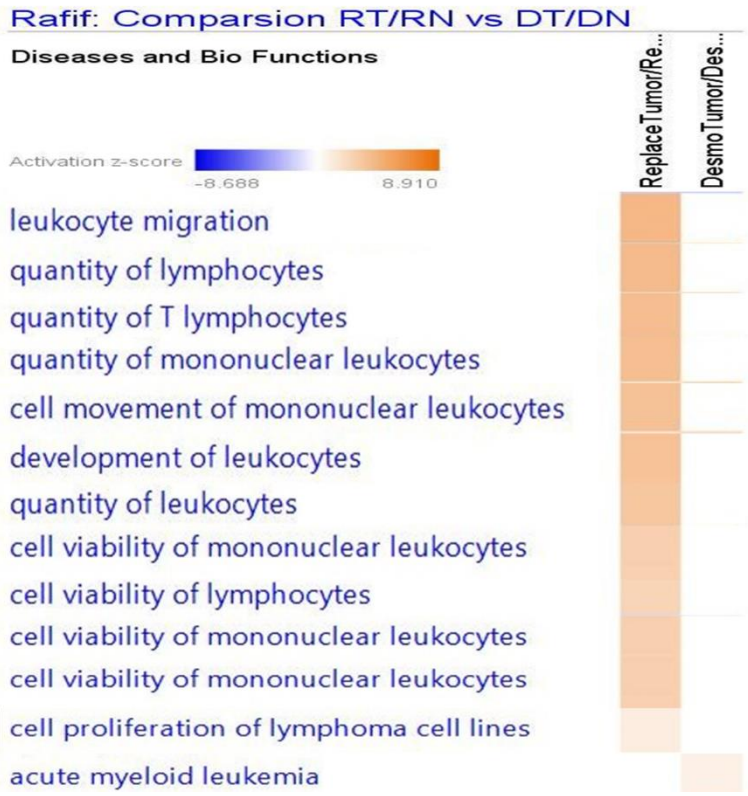

Quantification of T-lymphocytes and Macrophages

Patient Clinical and Pathological Features Data

Patient demographics and clinical data are summarized in (**Table 3**). Resected liver lesions from the 6 patients were included, 3 were desmoplastic and 3 replacement. All included liver lesions were at least 80% of the designated HGP. Four of the 6 patients were well-differentiated tumors, 2 of which contained mucin. The remaining 2 lesions were replacement and were moderately differentiated. Four out of the six patients were male. Their mean age was 64 years, with a range of 39-77 years. Only 2 patients had a rectal primary cancer, the remainder had colon cancers. Patients were followed up for an average of 72.13 months (32.53-148.83 months). Half presented with synchronous liver metastases, whereas the other half presented with metachronous lesions. The mean time between diagnosis of the primary and the liver metastases resection was 6.7 months (0.87-17.07 months) in the synchronous group, and 75.85 months (33.5-118.2 months) in

the metachronous group. One patient had a re-resection after 7 months for a recurrence. Two of our patients passed away, one following 30.6 months of his liver resection, and the other after 35.1 months.

Table 3. Patient Clinical Data.

Liver Tumor HGP	HGP%	Tumor differentiation	Gender	Age	Diagnosis of Primary	Site of Primary	Sync/ Meta	Liver Resection	Date of Death	Last Follow Up
Desmoplastic 1	95%	Well	F	72	01/10/2013	Colon	Sync	06/12/2013	-	17/06/2016
Desmoplastic 2	80%	Well w/ mucin	M	77	01/03/2004	Colon	Meta	07/01/2014	26/07/2016	26/07/2016
Desmoplastic 3	100%	Well w/ mucin	M	66	NA	Rectum	Meta	23/02/2012	27/01/2015	27/01/2015
Replacement 1	100%	Moderate	M	72	02/07/2009	Colon	Meta	17/04/2012	-	07/11/2016
Replacement 2	95%	Well	F	59	25/01/2012	Rectum	Sync	27/06/2013 21/01/2014	-	07/11/2016
Replacement 3	95%	Moderate	M	39	01/02/2014	Colon	Sync	27/02/2014	-	22/11/2016

Immune Cell Populations within the Desmoplastic HGP

Each immune subpopulation was contrasted between the 5 different areas of the desmoplastic sections.

Macrophages: (**Figs. 12 a-b**) Both $CD68^+$ $IRF5^+$ (M1 macrophages) and $CD68^+$ $CMAF^+$ cells (M2 macrophages) were highest in the desmoplastic ring, although only M2 macrophages reached statistical significance ($p = 0.0088$).

T-Lymphocytes: (**Figs. 12 c-d**) $CD4^+$ $FOXP3^+$ ($CD4^+$ regulatory T-lymphocytes), $CD4^+$ GZB^+ (cytotoxic helper T-lymphocytes), and $CD4^+$ GZB^- cells (helper T-lymphocytes) were also most abundant in the desmoplastic ring ($p = 0.0127$, 0.0068, and 0.0179, respectively). We identified an interesting immune cell subtype that is rarely discussed in the literature, $CD4^-$ $FOXP3^+$ cells, or in other words $CD4^-$ regulatory T-lymphocytes. We found them to be highest in the center of desmoplastic tumors, followed closely by the peripheries of the tumors ($p = 0.0098$).

Figure 12. Immune Cell Populations within the Desmoplastic HGP. Each subtype is compared by region (* $p < 0.05$). (**A, B**) Both $CD68^+$ $IRF5^+$ (M1 macrophages) and $CD68^+$ $CMAF^+$ cells (M2 macrophages) were highest in the desmoplastic ring, although only M2 macrophages reached statistical significance. (**C, D**) $CD4^+$ $FOXP3^+$ ($CD4^+$ regulatory T-lymphocytes), $CD4^+$ GZB^+ (cytotoxic helper T-lymphocytes), and $CD4^+$ GZB^- cells (helper T-lymphocytes) were also most abundant in the desmoplastic ring. $CD4^-$ $FOXP3^+$ cells, were found to be highest in the center of desmoplastic tumors, followed closely by the peripheries of the tumors.

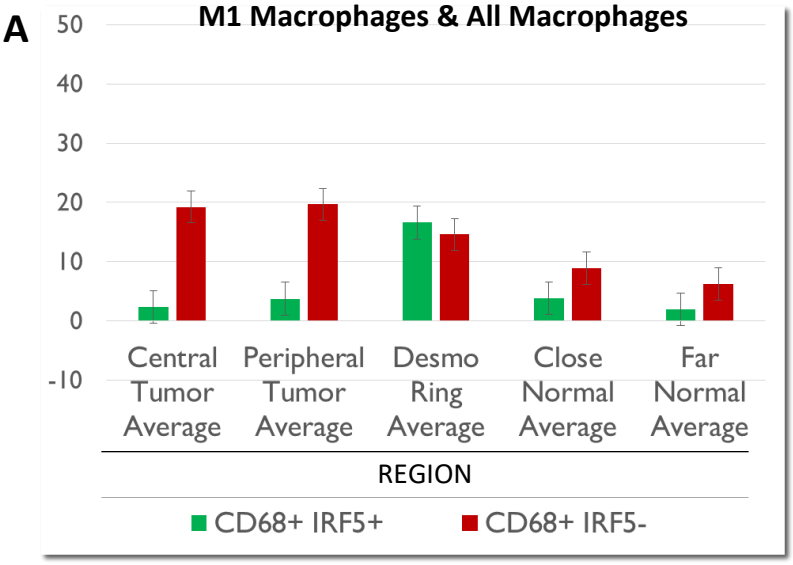

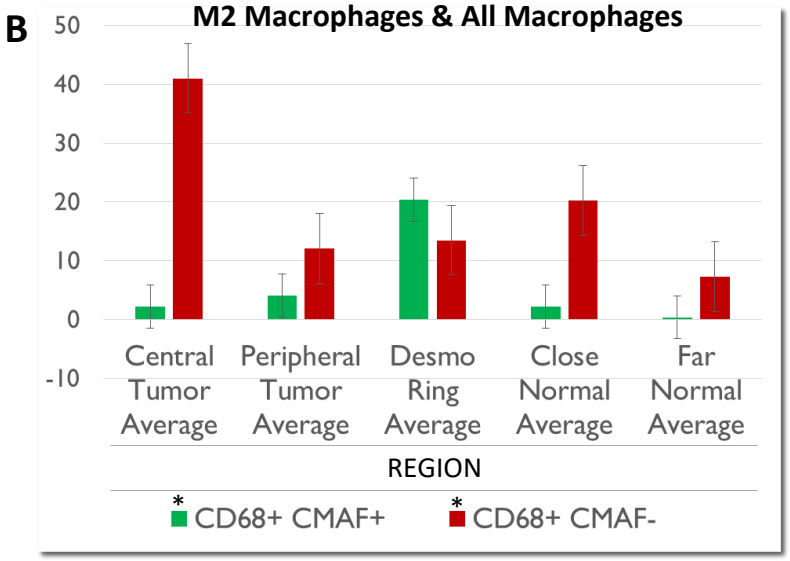

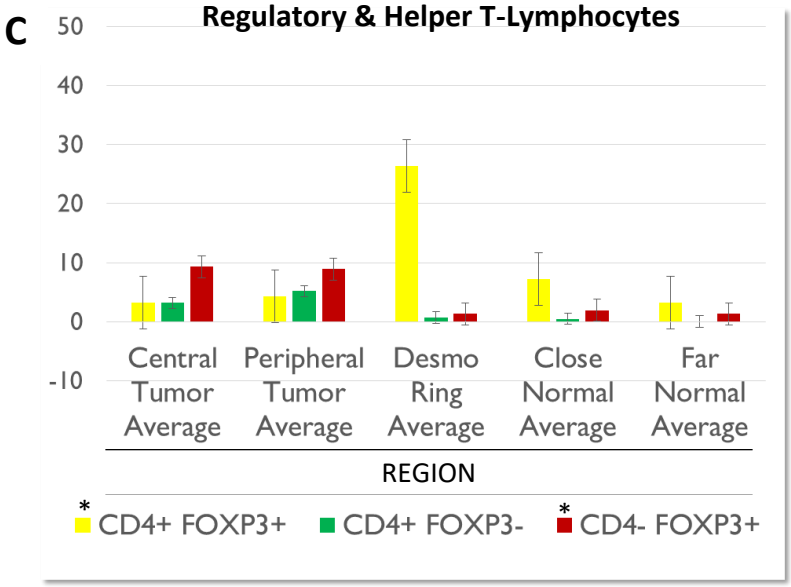

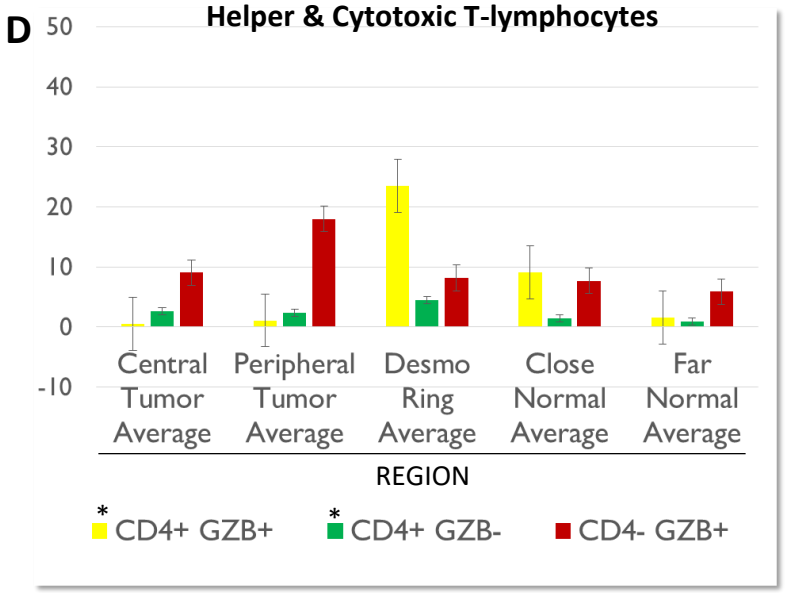

Immune Cell Populations within the Replacement HGP

Each immune subpopulation was contrasted between the 4 different areas of the replacement sections. Notably, there is not desmoplastic ring in this pattern. The column was left empty for convenience.

Macrophages: (**Figs. 13 a-b**) Both the M1 and M2 subtypes were concentrated at the tumor/liver interface, although M1s were higher in the peripheries of the tumors themselves ($p = 0.0155$), whereas M2s were highest in the normal livers adjacent to the tumors ($p = 0.001$).

T-Lymphocytes: (**Figs. 13 c-d**) $CD4^-$ regulatory T-lymphocytes and activated cytotoxic T-lymphocytes exhibited a similar trend ($p = 0.0009$ and 0.0011, respectively), they were most abundant in the tumors themselves, especially the peripheries. Second to which came the adjacent normal liver areas.

Figure 13. Immune Cell Populations within the Replacement HGP. Each subtype is compared by region (* $p < 0.05$). Note there is no desmoplastic ring in the replacement lesion. (**A, B**) Both the M1 and M2 subtypes were concentrated at the tumor/liver interface, although M1s were higher in the peripheries of the tumors themselves, whereas M2s were highest in the normal livers adjacent to the tumors. (**C, D**) $CD4^-$ regulatory T-lymphocytes and activated cytotoxic T-lymphocytes exhibited a similar trend they were most abundant in the tumors themselves, especially the peripheries. Second to which came the adjacent normal liver areas.

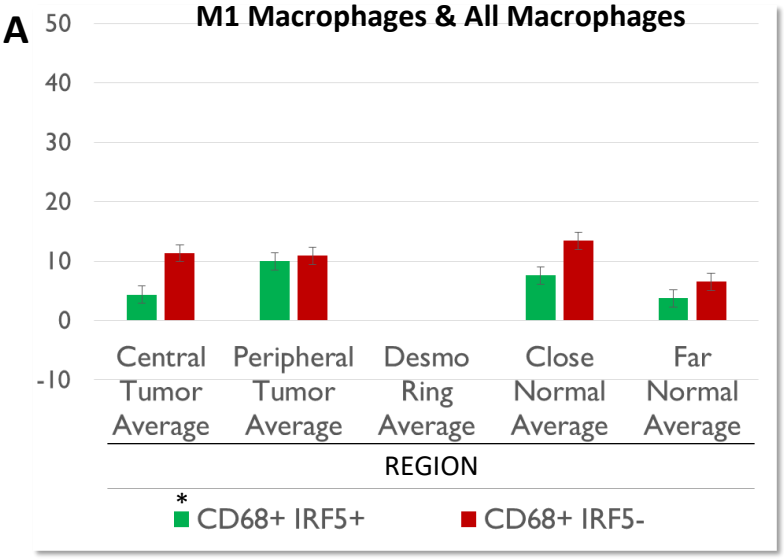

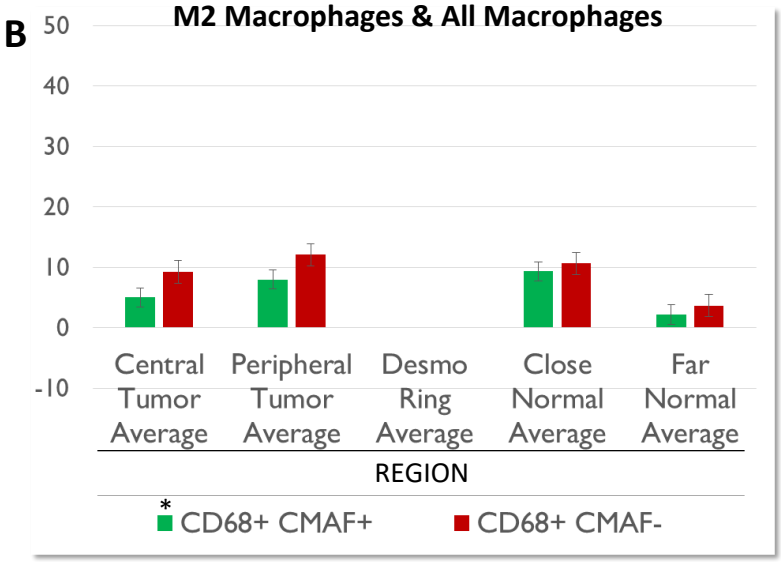

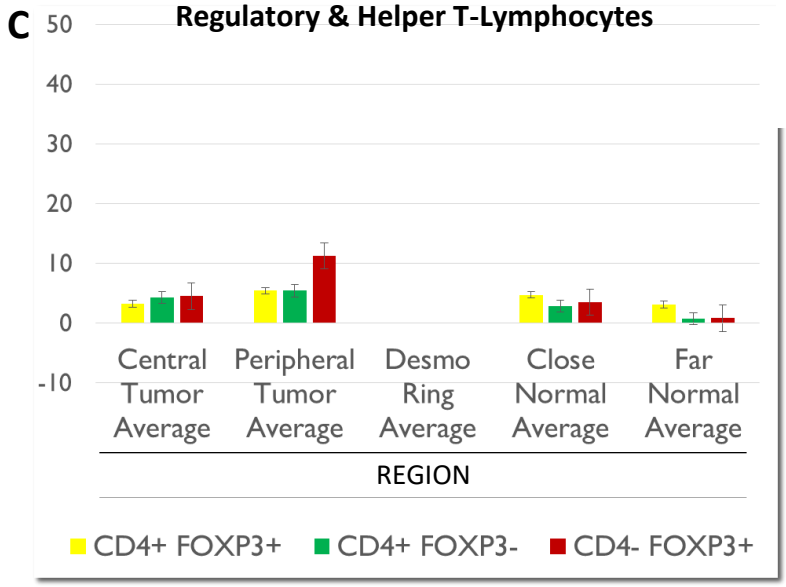

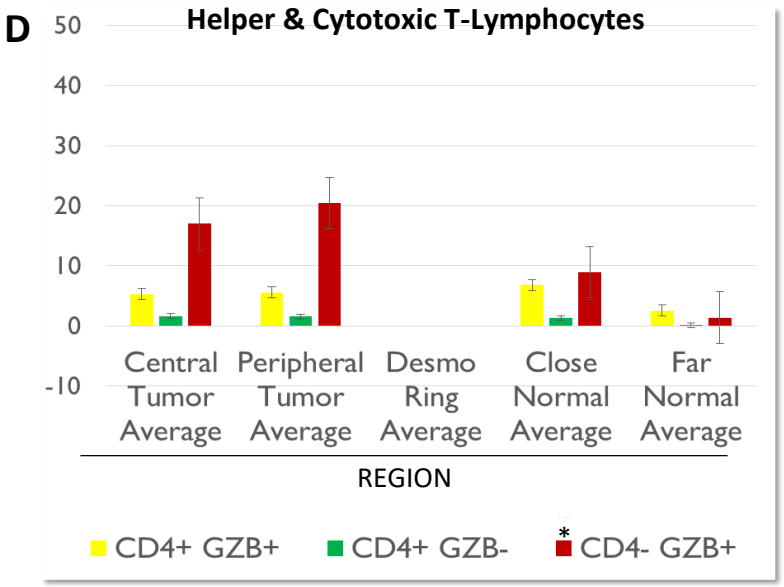

Comparison of Immune Cell Populations between Both HGPs

Each immune cell subtype was compared between the regions of each growth pattern. For example, numbers of M1 macrophages for were compared between the central tumor regions of the desmoplastic and replacement lesions.

1. $CD68^+$ $IRF5^+$ (M1 macrophages): they are more abundant in replacement lesions than in desmoplastic lesions, namely 2.67x higher in the tumor peripheries and almost twice as high in the far normal livers ($p = 0.0268$ and 0.0155, respectively) (**Fig. 14a**).
2. $CD68^+$ $IRF5^-$ (all macrophages): there were no statistically significant differences between both HGPs (**Fig. 14b**).
3. $CD68^+$ $CMAF^+$ (M2 macrophages): there are higher numbers in replacement lesions than in desmoplastic lesions, specifically twice as many in the tumor peripheries, more than 4x more in the adjacent normal livers, and more than 5x more in the far normal livers ($p = 0.0474$, 0.0013, and 0.0285, respectively) (**Fig. 14c**).
4. $CD68^+$ $CMAF^-$ (all macrophages): there were more in desmoplastic lesions than replacement lesions; precisely more than 4x more in the center of the tumor, and twice as many in the far normal livers ($p = 0.0142$) (**Fig. 14d**).
5. $CD4^+$ $FOXP3^+$ ($CD4^+$ regulatory T-lymphocytes): There were no statistically significant differences between both HGPs (**Fig. 14e**).
6. $CD4^+$ $FOXP3^-$ (helper T-lymphocytes): there are 5.66x more in the adjacent normal livers surrounding replacement tumors, than surrounding desmoplastic tumors ($p = 0.0445$) (**Fig. 14f**).
7. $CD4^-$ $FOXP3^+$ ($CD4^-$ regulatory T-lymphocytes): there are no statistically significant differences between both HGPs (**Fig. 14g**).
8. $CD4^+$ GZB^+ (cytotoxic helper T-lymphocytes): they are more abundant in replacement than in desmoplastic tumors, namely 10.66x more in the central tumor regions, and more than 5x more in the tumor peripheries ($p = 0.0272$ and 0.0018, respectively) (**Fig. 14h**).
9. $CD4^+$ GZB^- (helper T-lymphocytes): there are 11.5x more in the far normal livers surrounding desmoplastic lesions than surrounding replacement lesions ($p = 0.0155$) (**Fig. 14i**).
10. $CD4^-$ GZB^+ (activated cytotoxic T-lymphocytes): they are more than 4x more abundant in the far normal livers surrounding desmoplastic lesions than surrounding replacement

lesions (p = 0.0183) (**Fig. 14j**). In contrast, activated cytotoxic T-lymphocytes are highly upregulated in the central and peripheral tumors. There is a clear increase in both and a trend of higher levels in the replacement over desmoplastic, though this did not reach statistical significance.

Figure 14. Comparison of Immune Cell Populations between Both HGP (* p < 0.05). Of note that the "desmo ring" bar should be ignored in these figures, as the ring itslef is absent in the replacement type, and thus cannot be compared. (**A-D**) Macrophage populations. (**E-J**) T-lymphocyte populations.

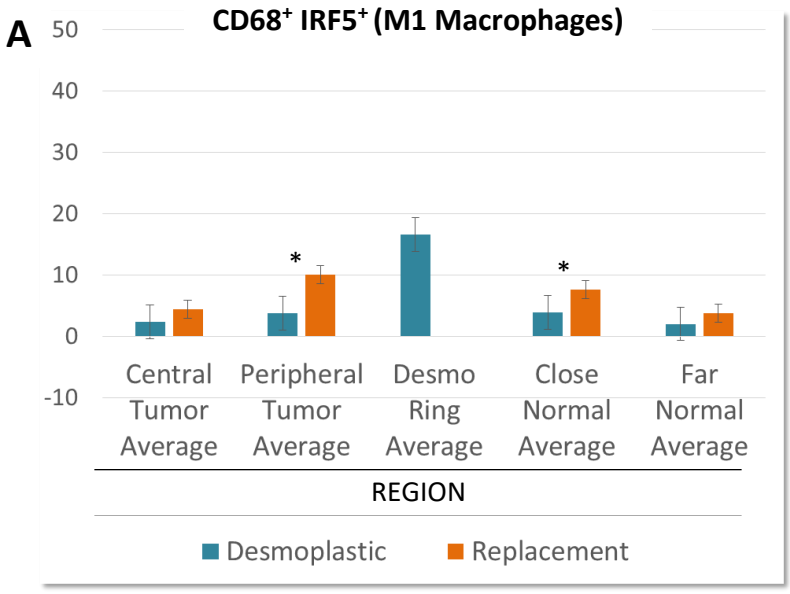

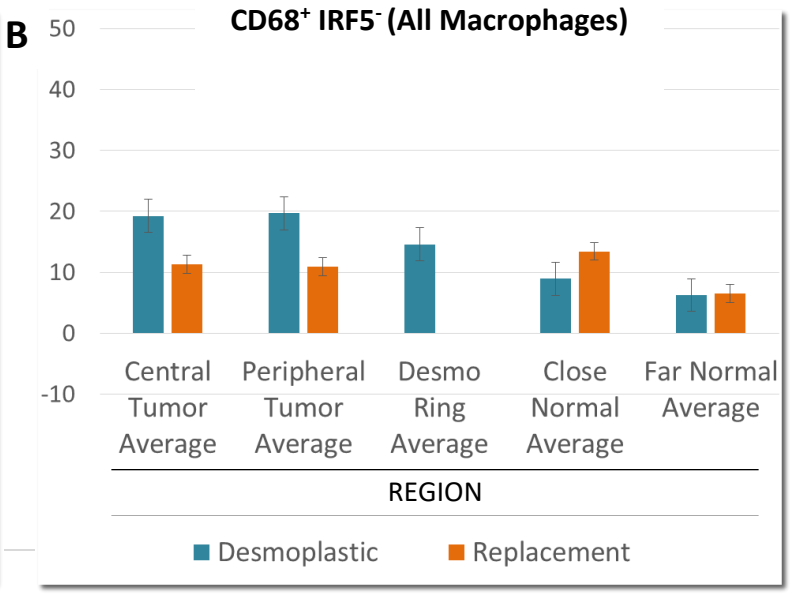

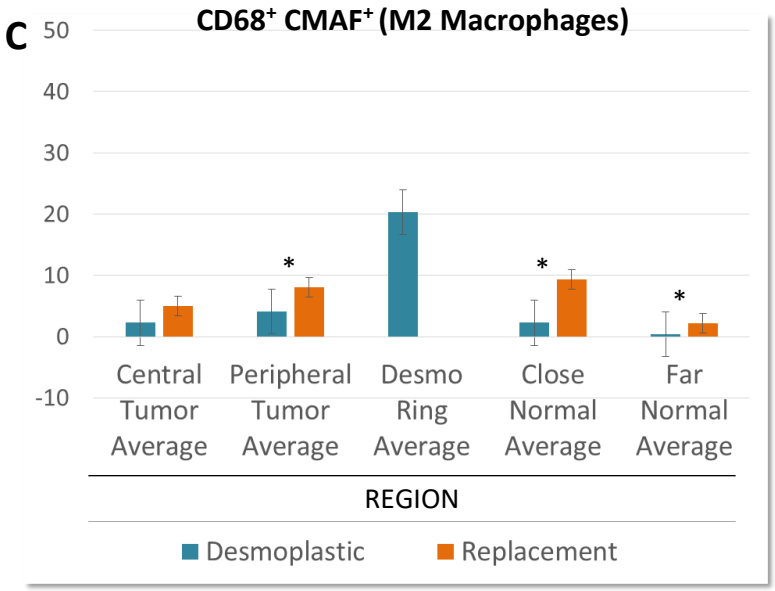
C
CD68+ CMAF+ (M2 Macrophages)
50
40
30
20
10
0
-10
*
*
*
Central Tumor Average
Peripheral Tumor Average
Desmo Ring Average
Close Normal Average
Far Normal Average
REGION
Desmoplastic
Replacement

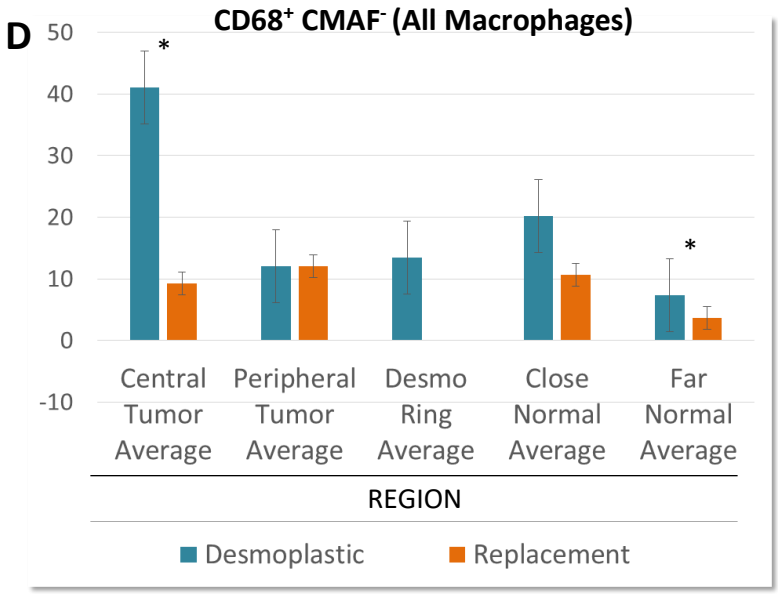
D
CD68+ CMAF- (All Macrophages)
50
40
30
20
10
0
-10
*
*
Central Tumor Average
Peripheral Tumor Average
Desmo Ring Average
Close Normal Average
Far Normal Average
REGION
Desmoplastic
Replacement

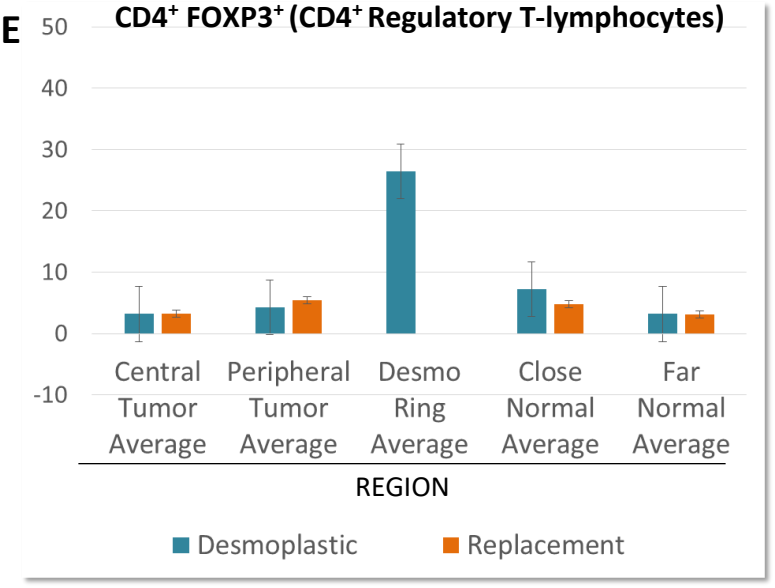
E
CD4+ FOXP3+ (CD4+ Regulatory T-lymphocytes)
50
40
30
20
10
0
-10
Central Tumor Average
Peripheral Tumor Average
Desmo Ring Average
Close Normal Average
Far Normal Average
REGION
Desmoplastic
Replacement

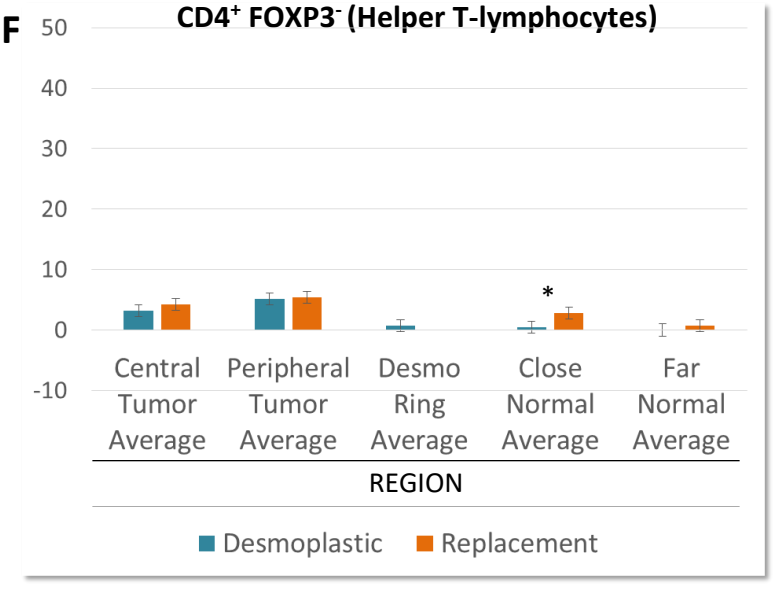
F
CD4+ FOXP3- (Helper T-lymphocytes)
50
40
30
20
10
0
-10
*
Central Tumor Average
Peripheral Tumor Average
Desmo Ring Average
Close Normal Average
Far Normal Average
REGION
Desmoplastic
Replacement

G

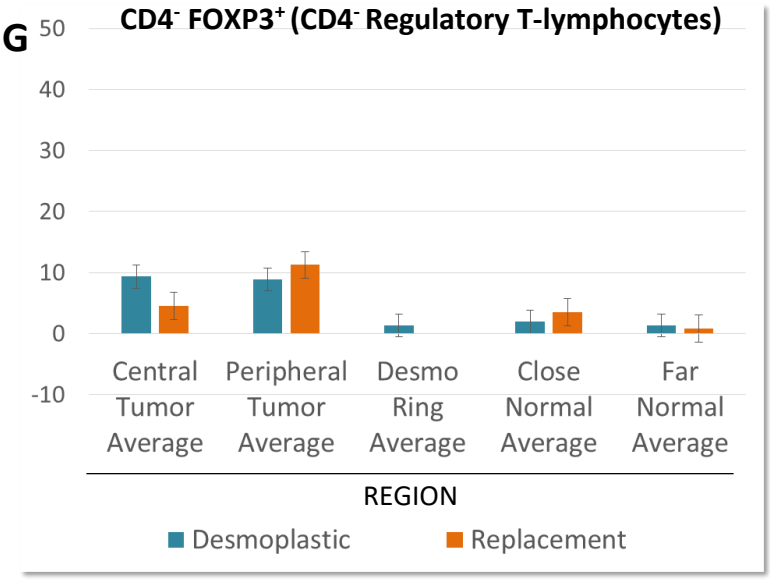
CD4- FOXP3+ (CD4- Regulatory T-lymphocytes)
50
40
30
20
10
0
-10
Central Tumor Average
Peripheral Tumor Average
Desmo Ring Average
Close Normal Average
Far Normal Average
REGION
Desmoplastic
Replacement

H

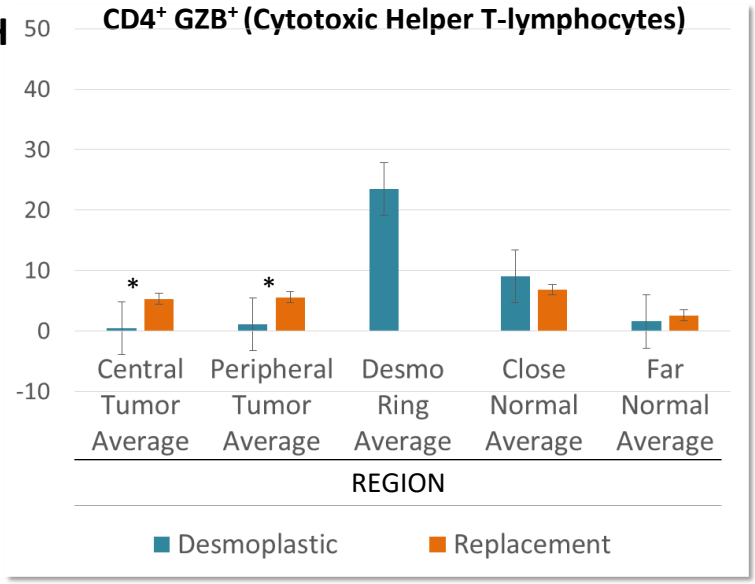
CD4+ GZB+ (Cytotoxic Helper T-lymphocytes)
50
40
30
20
10
0
-10
*
*
Central Tumor Average
Peripheral Tumor Average
Desmo Ring Average
Close Normal Average
Far Normal Average
REGION
Desmoplastic
Replacement

I

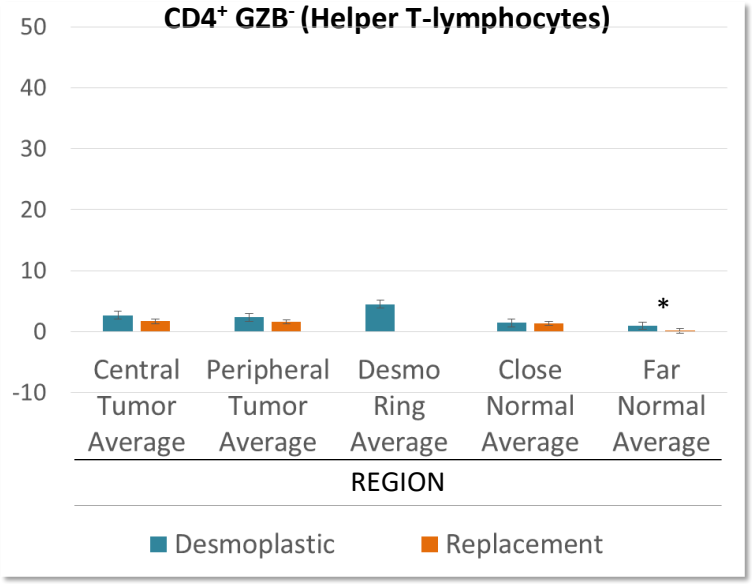
CD4+ GZB- (Helper T-lymphocytes)
50
40
30
20
10
0
-10
*
Central Tumor Average
Peripheral Tumor Average
Desmo Ring Average
Close Normal Average
Far Normal Average
REGION
Desmoplastic
Replacement

J

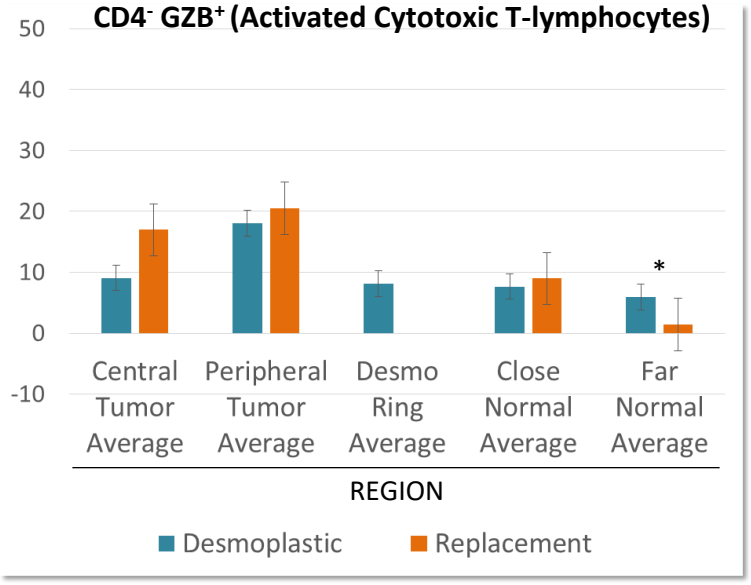
CD4- GZB+ (Activated Cytotoxic T-lymphocytes)
50
40
30
20
10
0
-10
*
Central Tumor Average
Peripheral Tumor Average
Desmo Ring Average
Close Normal Average
Far Normal Average
REGION
Desmoplastic
Replacement

Overall Infiltration of Immune Cells

To estimate and compare the level of inflammatory response between the two patterns, we calculated the overall infiltration of immune cells in the tissue sections, regardless of location (**Table 4**). In general, sections tended to have more macrophages than T-lymphocytes.

The desmoplastic patterns had a higher overall infiltration of macrophages than the replacement patterns. However, there was not an apparent difference in its M1 and M2 subtypes.

There was also a higher number of $CD4^+$ regulatory T-lymphocytes and cytotoxic helper T-lymphocytes in the desmoplastic patterns than in the replacements. In contrast, the replacement patterns had a higher overall infiltration of activated cytotoxic T-lymphocytes.

Table 4. Overall Infiltration of Immune Cells. (* $p < 0.05$)

Marker	Cell Type	Desmo. Average		Replace. Average	P-value
CD68+ IRF5+	M1 Macrophages	5.7	<	**6.42**	0.7321
CD68+ IRF5-	All Macrophages	**13.73**	>	10.54	0.3562
CD68+ CMAF+	M2 Macrophages	5.87	<	**6.13**	0.9061
CD68+ CMAF-	All Macrophages	**18.83**	>	8.92	0.0036*
CD4+ FOXP3+	CD4+ Regulatory T-lymphocytes	**8.83**	>	4.13	0.0855
CD4+ FOXP3-	Helper T-lymphocytes	1.9	<	**3.31**	0.1564
CD4- FOXP3+	CD4- Regulatory T-lymphocytes	4.57	<	**5.02**	0.7557
CD4+ GZB+	Cytotoxic Helper T-lymphocytes	**7.15**	>	5.08	0.416
CD4+ GZB-	Helper T-lymphocytes	**2.37**	>	1.17	0.0238*
CD4- GZB+	Activated Cytotoxic T-lymphocytes	9.76	<	**11.98**	0.4382

A Novel Subtype

Regulatory T-lymphocytes are generally considered to be a subtype of $CD4^+$ cells (also known as helper T-lymphocytes). Thus, a regulatory T-lymphocyte is expected to be $CD4^+$ $FOXP3^+$. We, however identified an immune cell subtype that is rarely mentioned in the literature; $CD4^-$ regulatory T-lymphocytes. Interestingly, we found this subtype in all regions of both desmoplastic and replacement lesions, including central tumor, peripheral tumor, desmoplastic ring, close normal liver, and far normal liver. This finding of $CD4^-$ regulatory T-lymphocytes is first to be reported by our study in both CRC and CRCLM patients.

Discussion

In our study, we contrasted the desmoplastic and replacement HGPs of CRCLM. Our data demonstrates that significant biological functions between the patterns consisted of those mostly related to cellular processes such as survival and invasion, suggesting that genes differentially expressed are those related to the tumor formation and metastases cascade. Furthermore, various genes that are related to immunological functions are mostly activated in the replacement pattern and conversely undetected in the desmoplastic subtypes. This led us to our second objective; quantification of immune cells between both patterns.

The majority of immune cell populations concentrated at the tumor/liver interface in both growth patterns, whether that be the tumor peripheries, the desmoplastic ring, or the adjacent normal livers. Furthermore, when comparing desmoplastic and replacement patterns, we found that immune cells are mostly higher at the tumor/liver interface of the replacement pattern. We have also identified a rare subtype of immune cells; CD4- regulatory T-lymphocytes. This population has not yet been described in patients with CRC or with CRCLM.

The liver is the destination of metastases from multiple malignancies. The presence of these liver metastases is more importantly a major determinant of survival. LM is commonly referred to as a unified entity, but the discovery and study of the 3 different HGPs, desmoplastic, replacement, and pushing, shed light on the diversity that exists between them. The patterns have been described in liver metastases of multiple cancers, including CRC. In 1996, an autopsy based study of metastatic liver lesions revealed that in liver metastases originating from lung, colon and pancreatic cancers, a replacement growth pattern prevailed [68]. In contrast to lesions metastasizing from gastric, gallbladder, and bile duct cancers, which the authors describe as "predominantly a sinusoidal growth pattern". In a more recent study by Ciolofan et al. [69], they confirm that all liver metastases from pancreatic primaries were of a replacement pattern, whereas those of a gastric origin displayed a pushing pattern. Our group has also previously identified these patterns in liver metastases from breast cancer, where the predominant type was replacement, with only a small minority identifying as desmoplastic lesions [16]. We continue to study the prevalence of each growth pattern in an array of malignancies.

Transcriptome of Desmoplastic and Replacement CRCLM

In our current RNA-seq analysis of CRCLM, we found that the gene signature of the 2 HGPs separated out clearly into two arms. Within the desmoplastic arm however, there were 2 samples that seemed to always create an additional subgroup within the greater arm of desmoplastic lesions. The biology of these 2 samples in specific needs to be looked at closely to understand the reasons behind this difference, as there could be further subgroups of patterns within the original desmoplastic pattern.

One of the most significantly expressed genes when comparing RT to RN by p-values was HSD17B13 (hydroxysteroid 17-beta dehydrogenase 13). It is involved in the process of lipid synthesis [70]. A gene differentially expressed in the expression heatmap was TF (transferrin). It is involved in the transport of iron molecules and regulation of endocytosis-related clearing of allergens in the bloodstream [71, 72]. Both genes are usually highly expressed in the liver [73]. This is in parallel to our data, as both these genes are highly expressed in our normal liver samples, in contrast to the replacement tumors where they are very minimal.

When comparing DT to DN by p-values, one of the most significantly expressed genes was AKR1C4 (aldo-keto reductase family 1 member C4), which it is involved in the conversion of various aldehydes and ketones into alcohols, this is important in the metabolism of steroids and androgens for instance [74, 75]. A gene differentially expressed in the expression heatmap was AMBP (alpha-1-microglobulin/bikunin precursor), which is involoved in regulation of the inflammatory process [76]. Both genes are also normally highly expressed in the liver [73]. This is also in parallel to our data, as both these genes are highly expressed in our normal liver samples, in contrast to the desmoplastic tumors where they are very minimal. As for the two DT samples that crossed over to the DN side, this could be due to the fact that as appose to microdissection, when using macrodissection as we did in our methodology, stromal cell contamination may occur. The two DT samples with a gene expression profile similar to DN may be contaminated.

One of the most significantly expressed genes when comparing RT to DT by p-values was CRP (C-reactive protein). This is a famous acute phase response marker, and is involved in various processes due to its ability to detect pathogens and damaged cell [77]. Our data shows that CRP is highly expressed in RT and only minimally in DT. This could be explained by our hypothesis that RT has an internal inflammatory response that counteracts the host's immune system, this

internal response may be absent in DT. Another explanation could be due to the fact that when the RT "replaces" hepatocytes, some normal liver cells interlace and remain in between the cancer cells (experiments done in our lab, data not shown). And as CRP is highly expressed in the liver [73], when macrodissecting, normal liver tissue was also included in the RT samples. The two DT that crossed over to the RT side could also be contaminated by normal liver, and thus contained high levels of CRP.

Although non-supervised clustering separated RN and DN from each other in the p-value heatmaps, no specific genes can be seen that are differentially expressed in a uniform manner. It seems that the normal livers surrounding both HGPs are similar.

We then found that canonical pathways and biological functions are never completely reversed between the 2 HGPs; functions are either up/down-regulated in both patterns but to a different extent, or absent all together. Significant biological functions between the patterns consisted of those mostly related to cellular processes such as survival and invasion, suggesting that genes differentially expressed are those related to the tumor formation and metastases cascade. Furthermore, various genes that are related to immunological functions are mostly activated in the replacement pattern and conversely undetected in the desmoplastic. This could also be explained by our hypothesis of the internal inflammatory response within the RT that counteracts the host's immune system, a response which may be absent in the DT.

In a matched transcriptome comparison by Lee et al. [78] the authors found that gene hierarchical clustering separated CRC and its liver metastases from normal colon and liver. However the primary CRC also clustered with the liver metastases, suggesting a high similarity in gene expression. The authors also performed a functional enrichment analysis, similar to our results, "cell cycle", "cell division", and "cellular process" were most significant. RNA-seq was also performed on syngeneic mice, comparing a CRC cell line to the formed liver metastases after inoculation, and also to the matched normal liver [79]. Genes clustered clearly into the 3 groups. Likewise, the top biological processes that came up were "inflammation", "angiogenesis", and "signal transduction". To our knowledge, we are the first to describe a transcriptome analysis of CRCLM describing and comparing the desmoplastic and replacement HGPs.

Immune Cell Populations of Desmoplastic and Replacement CRCLM

Subsequently, we have identified and quantified 10 immune cell subtypes in the desmoplastic and replacement HGPs of CRCLM. In the desmoplastic lesions, 4 populations were concentrated in the desmoplastic ring; M2 macrophages, $CD4^+$ regulatory T-lymphocytes, cytotoxic helper T-lymphocytes, and helper T-lymphocytes ($CD4^+$ GZB^-). Two populations were concentrated in the center of the desmoplastic tumor; all macrophages ($CD68^+$ $CMAF^-$) and $CD4^-$ regulatory T-lymphocytes. As a general rule, the second highest concentration is in the tumor/liver interface regions, i.e. the tumor peripheries and adjacent normal livers surrounding the tumors.

In the replacement lesions 4 populations show up as significant, two of which were also significant in the desmoplastic lesions. M1 and M2 macrophages are concentrated at the tumor/liver interface; M1s are higher in the peripheries of the replacement tumors themselves, whereas M2s are highest in the normal livers adjacent to the tumors. $CD4^-$ regulatory T-lymphocytes and activated cytotoxic T-lymphocytes exhibit a similar trend; they are most abundant in the replacement tumors themselves, especially the peripheries. Second to which come the central tumors, then the adjacent normal liver regions.

When comparing the 2 HGPs, twelve immune cell subtypes are significantly different between them (**Fig. 15** and **Table 5**). Immune cells are mostly higher in the replacement pattern, especially at the tumor/liver interface. This applies to both types of polarized macrophages (M1 and M2). As well as cytotoxic helper T-lymphocytes which specifically concentrate in the tumor peripheries, and helper T-lymphocytes ($CD4^+$ $FOXP3^-$) in the adjacent normal liver regions. The story is slightly different as we move farther away from the interface towards the central tumors and normal livers farthest from the tumors. Cytotoxic helper T-lymphocytes and M2 macrophages are higher in these regions in the replacement type, thus following a similar trend to what they had in the interface. However, we notice that most subtypes are actually higher in the desmoplastic lesions, namely all macrophages ($CD68^+$ $CMAF^-$) in the centers, additionally both activated cytotoxic T-lymphocytes and helper T-lymphocytes (that are $CD4^+$ GZB^-) in the normal livers farthest from the tumors. Noticeably, activated cytotoxic T-lymphocytes are highly upregulated in the central and peripheral tumors of both HGPs. There is a clear increase in both, and a trend of higher levels in the replacement over desmoplastic. Although this did not reach statistical significance, this probably due to the small sample size, and can be overcome by

increasing the numbers in the future. This also applies to $CD4^-$ regulatory T-lymphocytes at the peripheries of replacement tumors. $CD4^+$ regulatory T-lymphocytes however, displayed a higher trend in the normal areas surrounding the desmoplastic tumors. Although both are $FOXP3^+$, this could indicate that they might have contrasting roles. We also noticed that in some specimens, CD68+CMAF- differed in number than CD68+IRF5-, although they are meant to be the same cell type. Although we aimed to obtain serial sections for staining to allow contrasting of the different subtypes, sometimes a section was missing and a near cut was substituted. This could be the reason behind the difference.

Figure 15: Significant Immune Cell Populations between Both HGPs. Each marker is placed in the region which it is higher in. Markers colored in blue text indicate that they are higher in that region in desmoplastic lesions. Markers colored in orange text indicate that they are higher in that region in replacement lesions.

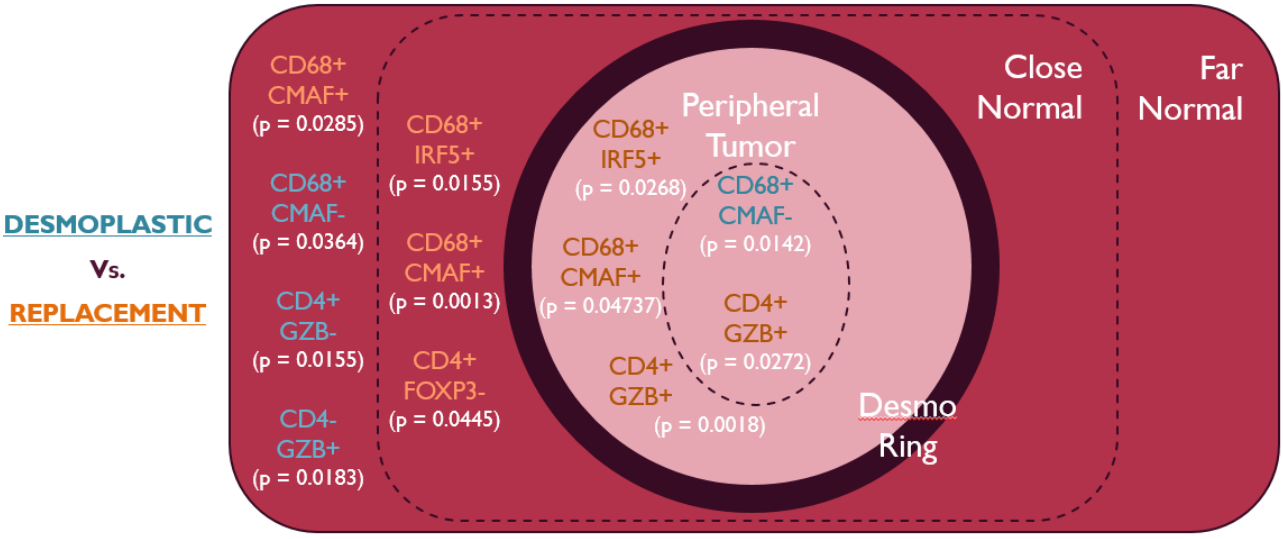

Table 5. Significant Immune Cell Populations between Both HGPs organized by region.

Region	Marker	Cell Type	Desmo. Average		Replace. Average	P-value
Central Tumor	CD68+ CMAF-	All Macrophages	**41**	>	9.25	0.0142
	CD4+ GZB+	Cytotoxic Helper T-Lymphocytes	0.5	<	**5.33**	0.0272
Peripheral Tumor	CD68+ IRF5+	M1 Macrophages	3.75	<	**10**	0.0268
	CD68+ CMAF+	M2 Macrophages	4.08	<	**8**	0.0474
	CD4+ GZB+	Cytotoxic Helper T-Lymphocytes	1.08	<	**5.58**	0.0018
Close Normal	CD68+ IRF5+	M1 Macrophages	3.83	<	**7.58**	0.0155
	CD68+ CMAF+	M2 Macrophages	2.25	<	**9.93**	0.0013
	CD4+ FOXP3-	Helper T-Lymphocytes	0.5	<	**2.83**	0.0445
Far Normal	CD68+ CMAF+	M2 Macrophages	0.42	<	**2.17**	0.0285
	CD68+ CMAF-	All Macrophages	**7.33**	>	3.67	0.0364
	CD4+ GZB-	Helper T-Lymphocytes	**0.92**	>	0.08	0.0155
	CD4- GZB+	Activated Cytotoxic T-Lymphocytes	**5.92**	>	1.42	0.0183

When calculating the overall infiltrate between the two HGPS, tissues tended to have more macrophages than T-lymphocytes. The desmoplastic patterns had a higher overall infiltration of macrophages than the replacement patterns. They also had higher numbers of $CD4^+$ regulatory T-lymphocytes and cytotoxic helper T-lymphocytes. In contrast, the replacement patterns had higher numbers of activated cytotoxic T-lymphocytes. The remaining subtypes only showed a subtle difference.

Although the study of the immune system in CRCLM has been ongoing for some time, it is only very recently that its role has been investigated in the context of the different HGPs. Nielsen et al. [47] described the lymphocytic infiltrate at the tumor edges of desmoplastic lesions as being more dense than at the edges of the pushing and replacement patterns. Nevertheless, this difference did not influence survival. The authors however did not differentiate the different subtypes of lymphocytes. The following year, the same group quantified macrophages (CD68) and T-lymphocytes (CD3) present in the tumor/liver interface of the different HGPs, and contrasted them in various stages of treatment [48]. They found that in chemonaïve patients,

replacement lesions had more macrophages than pushing. In patients that had received chemotherapy, desmoplastic patterns had a higher density of macrophages than pushing lesions. Finally in the group that received chemotherapy plus bevacizumab, a lower infiltration of T-lymphocytes was observed in mixed lesions in comparison to the pushing pattern. Although we did not include pushing lesions in our study, we did segregate each of our tumors into 5 regions; (1) central tumor, (2) peripheral tumor, (3) desmoplastic ring (absent in the replacement lesions), (4) close normal liver, (5) far normal liver. Noticeably, the majority of immune cell populations concentrated at the tumor/liver interface in both growth patterns, whether that is the tumor peripheries, the desmoplastic ring, or the adjacent normal livers (**Figs. 12-14**). Also, when comparing desmoplastic and replacement patterns, we found that immune cells are mostly higher at the tumor/liver interface of the replacement pattern (**Fig. 15**).

We believe we are the first to describe the various subpopulations of T-lymphocytes and macrophages in CRCLM in the light of the HGPs. Specifically helper, regulatory, and cytotoxic T-lymphocytes, as well as M1 and M2 macrophages. The difference that we see in our data from that previously published could be explained by the fact that we used various markers to identify subpopulations of immune cells, in contrast to using only one marker that identifies all T-lymphocytes (CD3) and all macrophages (CD68). This subdivision is most likely the cause of this discrepancy. It is known that each subtype of T-lymphocytes and macrophages have various and sometimes contrasting roles. By choosing this method we are able to study each subtype separately.

We also identified a rare subtype of immune cells; $CD4^-$ regulatory T-lymphocytes. Interestingly, they were found in all regions of both tumor patterns and their normal livers. Regulatory T-lymphocytes are generally considered to be a subtype of $CD4^+$ cells (also known as helper T-lymphocytes). Thus, a regulatory T-lymphocyte is expected to be $CD4^+$ $FOXP3^+$. There is emerging literature describing $CD4^-$ $CD8^-$ regulatory T-lymphocytes, named double negative regulatory T-lymphocytes [80, 81]. They have been studied in transplant tolerance, as they eliminate anti-donor $CD4^+$ T-lymphocytes, $CD8^+$ T-lymphocytes, and B-lymphocytes, thus prolonging survival of the graft [80, 82-85]. They were also found to suppress $CD8^+$ T-cell mediated responses in infectious and autoimmune models [86, 87]. The description of $CD4^-$ regulatory T-lymphocytes is novel in the literature of both CRC and CRCLM.

Another possibility, is that these $CD4^{-}FOXP3^{+}$ cells are either regulatory B-lymphocytes or cancer cells. Lately, regulatory B-lymphocytes (or B-regs) are being studied increasingly; $FOXP3^{+}$ B-regs are a newly discovered subtype. They have been isolated from human peripheral blood [88], as well as being suggested as a player in the pathogenesis of some autoimmune diseases, such as rheumatoid arthritis and cow milk allergy [89-91]. Kim et al. [92] recently described the expression of FOXP3 in colorectal cancer cells. They also stated that a higher expression correlated with worse outcome. A subset of regulatory B-cells have also been found in liver metastases of CRC, though they were not stained with $FOXP3^{+}$ specifically [93].

Conclusions

We have identified various biological functions in the transcriptome of the HGPs of CRCLM, suggesting that genes differentially expressed are those related to the tumor formation and metastases cascade. Genes related to immunological functions are mostly activated in the replacement pattern and conversely undetected in the desmoplastic.

This lead us to find multiple clear differences of the subtypes of T-lymphocytes and macrophages in the different HGPs. Most immune cell populations concentrate at the tumor/liver interface in both growth patterns, whether that be the tumor peripheries, the desmoplastic ring, or the adjacent normal livers. The interface is also the region where the differences between the HGPs arise, as we found that multiple immune cells are mostly higher at the tumor/liver interface of the replacement pattern. The identification of $CD4^{-}$ regulatory T-lymphocytes in novel in both CRC and CRCLM.

Different components of the immune system play diverse roles in the desmoplastic and replacement patterns of CRCLM. We believe we are the first to report these interesting findings. For long, CRCLM have been approached as unified entity. This segregation based on HGPs could explain the conflicting results in the literature, as each pattern is clearly different within itself, as well as its surrounding environment. These results help increase our understanding of the diversity of liver metastases. In an era that witnesses new therapies that are based on manipulation of various components of the immune system, we hope to be able to improve our patient outcomes by identifying those who would benefit most from such treatments.

Limitations and Future Directions

Our study was limited by its small sample size, as well as the usage of only double staining. Our future directions include expanding sample numbers to confirm our findings. The use of fluorescence-activated cell sorting (FACS) can help quantitate immune cells more accurately. Further characterization of immune cell subtypes can be achieved with additional markers such as CD8, CD44, and CD25. In our present study, we investigated immune cell populations in chemonaïve lesions. The addition of patients treated with chemotherapy alone, or chemotherapy plus bevacizumab will allow us to understand the effect of each therapy on the tumor's surrounding immune system. We also hope to develop an animal model to use targeted therapies against significant immune cells, and subsequently move on to a human clinical trial, aiming to achieve a tailored and improved survival benefit.

References

1. Siegel R, Naishadham D, Jemal A. Cancer statistics, 2013. CA: a cancer journal for clinicians. 2013;63(1):11-30.
2. Cancer Incidence Report Saudi Arabia 2010 [Internet]. Saudi Cancer Registry. 2014 [cited 20 September 2015]. Available from: http://www.chs.gov.sa/Ar/mediacenter/NewsLetter/2010%20Report%20(1).pdf.
3. Pestana C, Reitemeier RJ, Moertel CG, Judd ES, Dockerty MB. The Natural History of Carcinoma of the Colon and Rectum. American journal of surgery. 1964;108(6):826-9.
4. Weiss L, Grundmann E, Torhorst J, Hartveit F, Moberg I, Eder M, et al. Haematogenous metastatic patterns in colonic carcinoma: an analysis of 1541 necropsies. J Pathol. 1986;150(3):195-203.
5. Hugh TJ, Kinsella AR, Poston GJ. Management strategies for colorectal liver metastases--Part I. Surg Oncol. 1997;6(1):19-30.
6. Hugh TJ, Kinsella AR, Poston GJ. Management strategies for colorectal liver metastases--Part II. Surg Oncol. 1997;6(1):31-48.
7. Manfredi S, Lepage C, Hatem C, Coatmeur O, Faivre J, Bouvier AM. Epidemiology and management of liver metastases from colorectal cancer. Ann Surg. 2006;244(2):254-9.
8. Choti MA, Sitzmann JV, Tiburi MF, Sumetchotimetha W, Rangsin R, Schulick RD, et al. Trends in long-term survival following liver resection for hepatic colorectal metastases. Ann Surg. 2002;235(6):759-66.
9. Brouquet A, Mortenson MM, Vauthey JN, Rodriguez-Bigas MA, Overman MJ, Chang GJ, et al. Surgical strategies for synchronous colorectal liver metastases in 156 consecutive patients: classic, combined or reverse strategy? J Am Coll Surg. 2010;210(6):934-41.
10. Brouquet A, Abdalla EK, Kopetz S, Garrett CR, Overman MJ, Eng C, et al. High survival rate after two-stage resection of advanced colorectal liver metastases: response-based selection and complete resection define outcome. J Clin Oncol. 2011;29(8):1083-90.
11. Stangl R, Altendorf-Hofmann A, Charnley RM, Scheele J. Factors influencing the natural history of colorectal liver metastases. Lancet (London, England). 1994;343(8910):1405-10.
12. Khatri VP, Petrelli NJ, Belghiti J. Extending the frontiers of surgical therapy for hepatic colorectal metastases: is there a limit? J Clin Oncol. 2005;23(33):8490-9.
13. Hughes KS, Simon R, Songhorabodi S, Adson MA, Ilstrup DM, Fortner JG, et al. Resection of the liver for colorectal carcinoma metastases: a multi-institutional study of patterns of recurrence. Surgery. 1986;100(2):278-84.
14. Nagtegaal ID, Quirke P, Schmoll HJ. Has the new TNM classification for colorectal cancer improved care? Nature reviews Clinical oncology. 2011;9(2):119-23.
15. Vermeulen PB, Colpaert C, Salgado R, Royers R, Hellemans H, Van Den Heuvel E, et al. Liver metastases from colorectal adenocarcinomas grow in three patterns with different angiogenesis and desmoplasia. J Pathol. 2001;195(3):336-42.
16. Frentzas S, Simoneau E, Bridgeman VL, Vermeulen PB, Foo S, Kostaras E, et al. Vessel co-option mediates resistance to anti-angiogenic therapy in liver metastases. Nature medicine. 2016;22(11):1294-302.
17. Roitt I, Brostoff J, Male D. Immunology. Mosby. 4th ed. London, England1996.
18. Stitis DP, Stobo JD, Wells JV. Basic and Clinical Immunology. 7th ed: Appleton and Lange; 1991.
19. Sakaguchi S, Sakaguchi N, Asano M, Itoh M, Toda M. Immunologic self-tolerance maintained by activated T cells expressing IL-2 receptor alpha-chains (CD25). Breakdown of a single mechanism of self-tolerance causes various autoimmune diseases. Journal of immunology (Baltimore, Md : 1950). 1995;155(3):1151-64.

20. Wang R, Song L, Han G, Wang J, Chen G, Xu R, et al. Mechanisms of regulatory T-cell induction by antigen-IgG-transduced splenocytes. Scandinavian journal of immunology. 2007;66(5):515-22.
21. Piao WH, Jee YH, Liu RL, Coons SW, Kala M, Collins M, et al. IL-21 modulates CD4+ CD25+ regulatory T-cell homeostasis in experimental autoimmune encephalomyelitis. Scandinavian journal of immunology. 2008;67(1):37-46.
22. Wang Y, Meng J, Wang X, Liu S, Shu Q, Gao L, et al. Expression of human TIM-1 and TIM-3 on lymphocytes from systemic lupus erythematosus patients. Scandinavian journal of immunology. 2008;67(1):63-70.
23. Duffield JS, Forbes SJ, Constandinou CM, Clay S, Partolina M, Vuthoori S, et al. Selective depletion of macrophages reveals distinct, opposing roles during liver injury and repair. The Journal of clinical investigation. 2005;115(1):56-65.
24. Ghavami S, Shojaei S, Yeganeh B, Ande SR, Jangamreddy JR, Mehrpour M, et al. Autophagy and apoptosis dysfunction in neurodegenerative disorders. Progress in neurobiology. 2014;112:24-49.
25. Majai G, Kiss E, Tarr T, Zahuczky G, Hartman Z, Szegedi G, et al. Decreased apopto-phagocytic gene expression in the macrophages of systemic lupus erythematosus patients. Lupus. 2014;23(2):133-45.
26. Mantovani A, Biswas SK, Galdiero MR, Sica A, Locati M. Macrophage plasticity and polarization in tissue repair and remodelling. J Pathol. 2013;229(2):176-85.
27. Heydtmann M. Macrophages in hepatitis B and hepatitis C virus infections. Journal of virology. 2009;83(7):2796-802.
28. Schwabe RF, Brenner DA. Mechanisms of Liver Injury. I. TNF-alpha-induced liver injury: role of IKK, JNK, and ROS pathways. American journal of physiology Gastrointestinal and liver physiology. 2006;290(4):G583-9.
29. Mantovani A, Sica A, Sozzani S, Allavena P, Vecchi A, Locati M. The chemokine system in diverse forms of macrophage activation and polarization. Trends in immunology. 2004;25(12):677-86.
30. Martinez FO, Helming L, Gordon S. Alternative activation of macrophages: an immunologic functional perspective. Annual review of immunology. 2009;27:451-83.
31. Sica A, Invernizzi P, Mantovani A. Macrophage plasticity and polarization in liver homeostasis and pathology. Hepatology (Baltimore, Md). 2014;59(5):2034-42.
32. Huang WC, Sala-Newby GB, Susana A, Johnson JL, Newby AC. Classical macrophage activation up-regulates several matrix metalloproteinases through mitogen activated protein kinases and nuclear factor-kappaB. PloS one. 2012;7(8):e42507.
33. Song E, Ouyang N, Horbelt M, Antus B, Wang M, Exton MS. Influence of alternatively and classically activated macrophages on fibrogenic activities of human fibroblasts. Cellular immunology. 2000;204(1):19-28.
34. Lopez-Navarrete G, Ramos-Martinez E, Suarez-Alvarez K, Aguirre-Garcia J, Ledezma-Soto Y, Leon-Cabrera S, et al. Th2-associated alternative Kupffer cell activation promotes liver fibrosis without inducing local inflammation. International journal of biological sciences. 2011;7(9):1273-86.
35. Gibbons MA, MacKinnon AC, Ramachandran P, Dhaliwal K, Duffin R, Phythian-Adams AT, et al. Ly6Chi monocytes direct alternatively activated profibrotic macrophage regulation of lung fibrosis. American journal of respiratory and critical care medicine. 2011;184(5):569-81.
36. Alfano M, Graziano F, Genovese L, Poli G. Macrophage polarization at the crossroad between HIV-1 infection and cancer development. Arteriosclerosis, thrombosis, and vascular biology. 2013;33(6):1145-52.
37. Hanahan D, Weinberg RA. The hallmarks of cancer. Cell. 2000;100(1):57-70.
38. Hanahan D, Weinberg RA. Hallmarks of cancer: the next generation. Cell. 2011;144(5):646-74.
39. Pardoll DM. The blockade of immune checkpoints in cancer immunotherapy. Nature reviews Cancer. 2012;12(4):252-64.

40. Noy R, Pollard JW. Tumor-associated macrophages: from mechanisms to therapy. Immunity. 2014;41(1):49-61.
41. Naito Y, Saito K, Shiiba K, Ohuchi A, Saigenji K, Nagura H, et al. CD8+ T cells infiltrated within cancer cell nests as a prognostic factor in human colorectal cancer. Cancer research. 1998;58(16):3491-4.
42. Katz SC, Pillarisetty V, Bamboat ZM, Shia J, Hedvat C, Gonen M, et al. T cell infiltrate predicts long-term survival following resection of colorectal cancer liver metastases. Annals of surgical oncology. 2009;16(9):2524-30.
43. Katz SC, Bamboat ZM, Maker AV, Shia J, Pillarisetty VG, Yopp AC, et al. Regulatory T cell infiltration predicts outcome following resection of colorectal cancer liver metastases. Annals of surgical oncology. 2013;20(3):946-55.
44. Pages F, Kirilovsky A, Mlecnik B, Asslaber M, Tosolini M, Bindea G, et al. In situ cytotoxic and memory T cells predict outcome in patients with early-stage colorectal cancer. J Clin Oncol. 2009;27(35):5944-51.
45. Kruse J, von Bernstorff W, Evert K, Albers N, Hadlich S, Hagemann S, et al. Macrophages promote tumour growth and liver metastasis in an orthotopic syngeneic mouse model of colon cancer. International journal of colorectal disease. 2013;28(10):1337-49.
46. Cui YL, Li HK, Zhou HY, Zhang T, Li Q. Correlations of tumor-associated macrophage subtypes with liver metastases of colorectal cancer. Asian Pacific journal of cancer prevention : APJCP. 2013;14(2):1003-7.
47. Nielsen K, Rolff HC, Eefsen RL, Vainer B. The morphological growth patterns of colorectal liver metastases are prognostic for overall survival. Mod Pathol. 2014;27(12):1641-8.
48. Eefsen RL, Engelholm L, Alpizar-Alpizar W, Van den Eynden GG, Vermeulen PB, Christensen IJ, et al. Inflammation and uPAR-Expression in Colorectal Liver Metastases in Relation to Growth Pattern and Neo-adjuvant Therapy. Cancer Microenviron. 2015;8(2):93-100.
49. Kell DB. The virtual human: Towards a global systems biology of multiscale, distributed biochemical network models. IUBMB life. 2007;59(11):689-95.
50. Westerhoff HV, Palsson BO. The evolution of molecular biology into systems biology. Nat Biotechnol. 2004;22(10):1249-52.
51. Okoniewski MJ, Miller CJ. Hybridization interactions between probesets in short oligo microarrays lead to spurious correlations. BMC bioinformatics. 2006;7:276.
52. Royce TE, Rozowsky JS, Gerstein MB. Toward a universal microarray: prediction of gene expression through nearest-neighbor probe sequence identification. Nucleic acids research. 2007;35(15):e99.
53. Boguski MS, Tolstoshev CM, Bassett DE, Jr. Gene discovery in dbEST. Science (New York, NY). 1994;265(5181):1993-4.
54. Gerhard DS, Wagner L, Feingold EA, Shenmen CM, Grouse LH, Schuler G, et al. The status, quality, and expansion of the NIH full-length cDNA project: the Mammalian Gene Collection (MGC). Genome research. 2004;14(10B):2121-7.
55. Nagalakshmi U, Wang Z, Waern K, Shou C, Raha D, Gerstein M, et al. The transcriptional landscape of the yeast genome defined by RNA sequencing. Science (New York, NY). 2008;320(5881):1344-9.
56. Cloonan N, Forrest AR, Kolle G, Gardiner BB, Faulkner GJ, Brown MK, et al. Stem cell transcriptome profiling via massive-scale mRNA sequencing. Nature methods. 2008;5(7):613-9.
57. Gentleman RC, Carey VJ, Bates DM, Bolstad B, Dettling M, Dudoit S, et al. Bioconductor: open software development for computational biology and bioinformatics. Genome biology. 2004;5(10):R80.
58. Anders S, Huber W. Differential expression analysis for sequence count data. Genome biology. 2010;11(10):R106.

59. Croce AC, De Simone U, Freitas I, Boncompagni E, Neri D, Cillo U, et al. Human liver autofluorescence: an intrinsic tissue parameter discriminating normal and diseased conditions. Lasers in surgery and medicine. 2010;42(5):371-8.
60. Croce AC, Ferrigno A, Santin G, Piccolini VM, Bottiroli G, Vairetti M. Autofluorescence of liver tissue and bile: organ functionality monitoring during ischemia and reoxygenation. Lasers in surgery and medicine. 2014;46(5):412-21.
61. Wolman M. Lipid pigments (chromolipids): their origin, nature, and significance. Pathobiology annual. 1980;10:253-67.
62. Viegas MS, Martins TC, Seco F, do Carmo A. An improved and cost-effective methodology for the reduction of autofluorescence in direct immunofluorescence studies on formalin-fixed paraffin-embedded tissues. European journal of histochemistry : EJH. 2007;51(1):59-66.
63. Beljaars L, Schippers M, Reker-Smit C, Martinez FO, Helming L, Poelstra K, et al. Hepatic Localization of Macrophage Phenotypes during Fibrogenesis and Resolution of Fibrosis in Mice and Humans. Front Immunol. 2014;5:430.
64. Barros MH, Hauck F, Dreyer JH, Kempkes B, Niedobitek G. Macrophage polarisation: an immunohistochemical approach for identifying M1 and M2 macrophages. PloS one. 2013;8(11):e80908.
65. Garnelo M, Tan A, Her Z, Yeong J, Lim CJ, Chen J, et al. Interaction between tumour-infiltrating B cells and T cells controls the progression of hepatocellular carcinoma. Gut. 2015.
66. Law JP, Hirschkorn DF, Owen RE, Biswas HH, Norris PJ, Lanteri MC. The importance of Foxp3 antibody and fixation/permeabilization buffer combinations in identifying CD4+CD25+Foxp3+ regulatory T cells. Cytometry Part A : the journal of the International Society for Analytical Cytology. 2009;75(12):1040-50.
67. Lazaris A, Amri A, Zoroquiain P, Petrillo SK, Mattar R, Gao Z-H, et al. Abstract 1695: Vascularization of colorectal cancer liver metastasis: correlation with growth patterns. Cancer research. 2016;76(14 Supplement):1695.
68. Terayama N, Terada T, Nakanuma Y. Histologic growth patterns of metastatic carcinomas of the liver. Jpn J Clin Oncol. 1996;26(1):24-9.
69. Ciolofan A, Ceausu RA, Cimpean AM, Pușa G, Stef DG, Cretu O, et al. The Interrelations between the Histological Growth Pattern and Angiogenesis in Liver Metastases of Gastric, Pancreatic or Colorectal Origin. Med Con. 2016;11(1):19-23.
70. Su W, Wang Y, Jia X, Wu W, Li L, Tian X, et al. Comparative proteomic study reveals 17beta-HSD13 as a pathogenic protein in nonalcoholic fatty liver disease. Proceedings of the National Academy of Sciences of the United States of America. 2014;111(31):11437-42.
71. Waheed A, Britton RS, Grubb JH, Sly WS, Fleming RE. HFE association with transferrin receptor 2 increases cellular uptake of transferrin-bound iron. Archives of biochemistry and biophysics. 2008;474(1):193-7.
72. Griffiths WJ, Cox TM. Co-localization of the mammalian hemochromatosis gene product (HFE) and a newly identified transferrin receptor (TfR2) in intestinal tissue and cells. The journal of histochemistry and cytochemistry : official journal of the Histochemistry Society. 2003;51(5):613-24.
73. Fagerberg L, Hallstrom BM, Oksvold P, Kampf C, Djureinovic D, Odeberg J, et al. Analysis of the human tissue-specific expression by genome-wide integration of transcriptomics and antibody-based proteomics. Molecular & cellular proteomics : MCP. 2014;13(2):397-406.
74. Qin KN, New MI, Cheng KC. Molecular cloning of multiple cDNAs encoding human enzymes structurally related to 3 alpha-hydroxysteroid dehydrogenase. The Journal of steroid biochemistry and molecular biology. 1993;46(6):673-9.
75. Khanna M, Qin KN, Wang RW, Cheng KC. Substrate specificity, gene structure, and tissue-specific distribution of multiple human 3 alpha-hydroxysteroid dehydrogenases. The Journal of biological chemistry. 1995;270(34):20162-8.

76. Berggard T, Enghild JJ, Badve S, Salafia CM, Logdberg L, Akerstrom B. Histologic distribution and biochemical properties of alpha 1-microglobulin in human placenta. American journal of reproductive immunology (New York, NY : 1989). 1999;41(1):52-60.
77. Mold C, Gewurz H, Du Clos TW. Regulation of complement activation by C-reactive protein. Immunopharmacology. 1999;42(1-3):23-30.
78. Lee JR, Kwon CH, Choi Y, Park HJ, Kim HS, Jo HJ, et al. Transcriptome analysis of paired primary colorectal carcinoma and liver metastases reveals fusion transcripts and similar gene expression profiles in primary carcinoma and liver metastases. BMC cancer. 2016;16:539.
79. Bocuk D, Wolff A, Krause P, Salinas G, Bleckmann A, Hackl C, et al. The adaptation of colorectal cancer cells when forming metastases in the liver: expression of associated genes and pathways in a mouse model. BMC cancer. 2017;17(1):342.
80. Ford MS, Zhang ZX, Chen W, Zhang L. Double-negative T regulatory cells can develop outside the thymus and do not mature from CD8+ T cell precursors. Journal of immunology (Baltimore, Md : 1950). 2006;177(5):2803-9.
81. Johansson M, Lycke N. A unique population of extrathymically derived alpha beta TCR+CD4-CD8- T cells with regulatory functions dominates the mouse female genital tract. Journal of immunology (Baltimore, Md : 1950). 2003;170(4):1659-66.
82. Zhang ZX, Yang L, Young KJ, DuTemple B, Zhang L. Identification of a previously unknown antigen-specific regulatory T cell and its mechanism of suppression. Nature medicine. 2000;6(7):782-9.
83. Ford MS, Young KJ, Zhang Z, Ohashi PS, Zhang L. The immune regulatory function of lymphoproliferative double negative T cells in vitro and in vivo. The Journal of experimental medicine. 2002;196(2):261-7.
84. Zhang ZX, Stanford WL, Zhang L. Ly-6A is critical for the function of double negative regulatory T cells. European journal of immunology. 2002;32(6):1584-92.
85. Ma Y, He KM, Garcia B, Min W, Jevnikar A, Zhang ZX. Adoptive transfer of double negative T regulatory cells induces B-cell death in vivo and alters rejection pattern of rat-to-mouse heart transplantation. Xenotransplantation. 2008;15(1):56-63.
86. Crispin JC, Tsokos GC. Human TCR-alpha beta+ CD4- CD8- T cells can derive from CD8+ T cells and display an inflammatory effector phenotype. Journal of immunology (Baltimore, Md : 1950). 2009;183(7):4675-81.
87. Riol-Blanco L, Lazarevic V, Awasthi A, Mitsdoerffer M, Wilson BS, Croxford A, et al. IL-23 receptor regulates unconventional IL-17-producing T cells that control bacterial infections. Journal of immunology (Baltimore, Md : 1950). 2010;184(4):1710-20.
88. Noh J, Choi WS, Noh G, Lee JH. Presence of Foxp3-expressing CD19(+)CD5(+) B Cells in Human Peripheral Blood Mononuclear Cells: Human CD19(+)CD5(+)Foxp3(+) Regulatory B Cell (Breg). Immune network. 2010;10(6):247-9.
89. Guo Y, Zhang X, Qin M, Wang X. Changes in peripheral CD19(+)Foxp3(+) and CD19(+)TGFbeta(+) regulatory B cell populations in rheumatoid arthritis patients with interstitial lung disease. J Thorac Dis. 2015;7(3):471-7.
90. Noh J, Noh G, Kim HS, Kim AR, Choi WS. Allergen-specific responses of CD19(+)CD5(+)Foxp3(+) regulatory B cells (Bregs) and CD4(+)Foxp3(+) regulatory T cell (Tregs) in immune tolerance of cow milk allergy of late eczematous reactions. Cellular immunology. 2012;274(1-2):109-14.
91. Park MK, Jung YO, Lee SY, Lee SH, Heo YJ, Kim EK, et al. Amelioration of autoimmune arthritis by adoptive transfer of Foxp3-expressing regulatory B cells is associated with the Treg/Th17 cell balance. Journal of translational medicine. 2016;14(1):191.
92. Kim M, Grimmig T, Grimm M, Lazariotou M, Meier E, Rosenwald A, et al. Expression of Foxp3 in colorectal cancer but not in Treg cells correlates with disease progression in patients with colorectal cancer. PloS one. 2013;8(1):e53630.

93. Shimabukuro-Vornhagen A, Schlosser HA, Gryschok L, Malcher J, Wennhold K, Garcia-Marquez M, et al. Characterization of tumor-associated B-cell subsets in patients with colorectal cancer. Oncotarget. 2014;5(13):4651-64.